Enhanced net CO2 exchange of a semi-deciduous forest in the southern Amazon due to diffuse radiation from biomass burning

Simone N. R. Silva[1], Glauber Cirino[1], Demerval Soares Moreira[2], Rafael Da Silva Palácios[1], Maria Isabel Vitorino[1], and George Louis Vourlitis[3]

[1]Federal University of Pará
[2]São Paulo State University
[3]California State University

January 16, 2023

Abstract

Atmospheric processes and climate are closely linked to the carbon cycle in the Amazon region as a consequence of the strong biosphere-atmosphere coupling. The radiative effects of aerosols and clouds are still unknown for a wide variety of species and types of vegetation present in Amazonian biomes. This study examines the effects of atmospheric aerosols on solar radiation and their effects on Net Ecosystem Exchange (NEE) in an area of semideciduous tropical forest in the North of Mato Grosso State. Our results show a reduction of assimilation in the NEE with a considerable loss with the decrease of incident solar radiation of 40% and relative irradiance between 1.10-0.67. An average increase of 35-70% in net CO2 assimilation was observed for pollution levels (Aerosol Optical Depth) above 1.25. The increase of 35-70% in the NEE was attributed to the increase of up to 60% in the diffuse fraction of Photosynthetically Active Radiation, concerning its direct fraction. These results were mainly attributable to the Biomass Burning Organic Aerosols from fires over the area studied. Important influences on temperature and relative humidity of air, induced by the interaction between solar radiation and high aerosol load in the observation area, were also observed; an average cooling of 3.0 °C and 10%, respectively. Given the long-distance transport of aerosols emitted by burning biomass, significant changes in CO2 flux can be occurring over large areas of the Amazon, with important effects on the potential for CO2 absorption on ecosystems of semideciduous forests distributed in the region.

Enhanced net CO_2 exchange of a semi-deciduous forest in the southern Amazon due to diffuse radiation from biomass burning

S. N. R. Silva[1], G. G. Cirino[2,1,5], D. S. Moreira[3], R. S. Palácios[2,5], M. I. Vitorino[1,2], and G. L. Vourlitis[4]

[1]Programa de Pós-Graduação em Ciências Ambientais, Universidade Federal do Pará, Belém-PA, Brazil
[2]Instituto de Geociências, Faculdade de Meteorologia, Universidade Federal do Pará, Belém-PA, Brazil
[3]Faculdade de Ciências, Universidade Estadual Paulista, Bauru-SP, Brazil
[4]Department of Biological Sciences, California State University, San Marcos, CA, USA
[5]Programa de Pós-Graduação em Gestão de Risco e Desastre na Amazônia, Universidade Federal do Pará, Belém-PA, Brazil

Key Points:

- Enhancement up to 40% in the diffuse PAR for high aerosols loading ($\mathsf{AOD} \geq 1.25$)
- Enhancement up to 20-70% in the NEE of CO_2 for high aerosols loading ($\mathsf{AOD} \geq 1.25$)
- Photosynthetic interruption for relative irradiance values below 60%
- Decrease in the NEE of CO_2 for canopy temperature values below 25 °C
- Decrease in the NEE of CO_2 for VPD values below 3-4 hPa

Corresponding author: G. L. Vourlitis, `georgev@csusm.edu`

Abstract

Atmospheric processes and climate are closely linked to the carbon cycle in the Amazon region as a consequence of the strong biosphere-atmosphere coupling. The radiative effects of aerosols and clouds are still unknown for a wide variety of species and types of vegetation present in Amazonian biomes. This study examines the effects of atmospheric aerosols on solar radiation and their effects on Net Ecosystem Exchange (NEE) in an area of semideciduous tropical forest in the North of Mato Grosso State. Our results show a reduction of assimilation in the NEE with a considerable loss with the decrease of incident solar radiation of $\approx 40\%$ and relative irradiance between 1.10-0.67. An average increase of 35-70% in net CO_2 assimilation was observed for pollution levels (Aerosol Optical Depth) above ≈ 1.25. The increase of 35-70% in the NEE was attributed to the increase of up to 60% in the diffuse fraction of Photosynthetically Active Radiation concerning its direct fraction. These results were mainly attributable to the Biomass Burning Organic Aerosols from fires over the area studied. Important influences on temperature and relative humidity of air induced by the interaction between solar radiation and high aerosol load in the observation area, were also observed; an average cooling of $\approx 3.0°C$ and 10%, respectively. Given the long-distance transport of aerosols emitted by burning biomass, significant changes in CO_2 flux can be occurring over large areas of the Amazon, with important effects on the potential for CO_2 absorption on ecosystems of semideciduous forests distributed in the region.

Plain Language Summary

Here, first we obtained clear-sky curves with the AOD measurements from the AERONET sun photometer network. Next this, the radiative effects of aerosols on the CO_2 fluxes for experimental site were analyzed. Measurements of NEE, total PAR radiation (PAR_i), diffuse PAR radiation (PAR_d), (AOD_a), (RH_{air}), (T_{air}) and surface temperature of the forest canopy (Td_f) were further analyzed as a function of the relative irradiance parameter (f), from July to November, during the burnig season in the region.

1 Introduction

1.1 Scientific Contextualization

Carbon is a key element in global biogeochemical cycles. Understanding its balance is fundamental to understanding the interactions between life (bio) the earth (geo) and chemistry. In the current context of global climate change, the modulating agents of CO_2 stocks and fluxes, especially through photosynthesis-respiration processes, have been widely debated (Booth et al., 2012; Huntingford et al., 2013; Brienen et al., 2015) with emphasis on the role of tropical forests, especially for the Amazon (Doughty et al., 2015; Braghiere, Kerches Renato, Akemi Yamasoe et al., 2020; Gatti et al., 2014, 2021). The result of increasing atmospheric CO_2 levels associated with climate change provides important feedback on the future of greenhouse warming (Booth et al., 2012; Huntingford et al., 2013).

In the Amazon biome, forest ecosystems play an important role in the dynamics between the carbon cycle of the terrestrial component and the climate, and even if these forests seem to have a uniform behavior, they have climatic sub-regions with peculiarities for the process of absorption and release of carbon (Brienen et al., 2015; Gatti et al., 2021). The absorption, carried out through photosynthesis, increases the stock of CO_2 fixed by the vegetation, incorporating this component as a biomass gain, that is, a carbon sink. The process of respiration of vegetation and soil releases CO_2 into the atmosphere, that is, a source of carbon for the atmosphere. Photosynthesis and respiration processes can vary considerably from sub-region to sub-region in Amazonia, resulting in distinct carbon source or sink behaviors depending on geographic location and climatic conditions (Doughty et al., 2015; Silva et al., 2020).

In general, the participation of forests in the global carbon cycle can only be adequately quantified by long-term studies monitoring carbon exchange at the plant-atmosphere interface. Forests participate in this cycling effectively, storing 200-300 Pg C (Pan, 2011; Saatchi et al., 2011; Avitabile et al., 2016), about a third of what is contained in the atmosphere. This stock is very dynamic and these trees process about 60% of global photosynthesis, sequestering about 72 Pg C from the atmospheric component every year (Beer et al., 2010), but also releasing a similar amount back into the atmosphere via respiration of plants and animals, microorganisms and fungi of the (R. C. Nagy et al., 2018) ecosystem. In these large fluxes, a small proportionate change in the uptake or release of CO_2 to the atmosphere can result in a large net source or sink.

Changes in carbon concentrations in the atmosphere since the industrial era directly impact the role of forest in carbon cycles, which can alternate between the source or sink of CO_2. Recent reports (Gatti et al., 2021) show that some regions of the Amazon act as a source of CO_2 to the atmosphere, as a result of logging, land use change, and fires that occur in the region. However, other research indicates that Amazonian forests can be net sinks for atmospheric CO_2 (Carswell et al., 2002; von Randow et al., 2004) or approximately in balance (Vourlitis et al., 2011). In general, the balance between the rates of carbon emission or fixation is delicate, so small external disturbances can change the dynamics of the forest and the state of the climate system.

Among the modulating agents of the CO_2 balance, solar radiation stands out, as a fundamental component for both photosynthesis and forest respiration. In Brazil, and especially in the Amazon region, the burning of biomass emits large amounts of gases and aerosols into the atmosphere, these emissions can strongly alter radiative fluxes, impacting CO_2 (Aragão et al., 2018; Malavelle et al., 2019; Morgan et al., 2019; de Magalhães et al., 2019). Atmospheric aerosols from biomass burning intimately affect the light use efficiency (LUE) and ecosystem productivity, influencing the solar radiation received in the system and other exogenous environmental conditions (Kanniah et al., 2012; Mercado et al., 2009). Studies of the effects of aerosols carried out on terrestrial ecosystems have found positive, negative, and neutral effects. In Amazonia, these effects were also observed in some regions, such as in the central part (G. G. Cirino et al., 2014), east (Doughty et al., 2010; Oliveira et al., 2007) and southwest (Yamasoe et al., 2006; G. G. Cirino et al., 2014), but remain unknown in critically important ecosystems, such as seasonal forests (in the region of the deforestation arc), Pantanal forests, woodlands and cerrado. Modeling studies have also demonstrated the impact of aerosols on gross primary production (GPP) on a regional (Moreira et al., 2013; Bian et al., 2021) and global (Mercado et al., 2009; Rap, 2015) scale.

The models used in these studies, however, need improvements in the physical parameterization of the radiative effects of aerosols and clouds, direct long-term observations in these ecosystems. These improvements are fundamental for more accurate and realistic spatialization of the potential for the absorption of atmospheric CO_2 by the Amazon as a whole (Aragão et al., 2018). In this sense, the potential for fire-induced atmospheric aerosols to impact to CO_2 absorption by the seasonal forest in Mato Grosso (in the region of the deforestation arc), has not yet been evaluated, either by direct observation or by numerical modeling. It is known that these tropical semideciduous forests play a central role in the terrestrial system, preserving biodiversity (Fu et al., 2018). This biome, located on the frontier of deforestation, is an excellent laboratory to assess the effects of exogenous factors on forest productivity, as it is under strong anthropic impact due to changes in land use, destined for the advancement of soy monoculture, livestock, and the timber industry, as well as high vulnerability to fire. These are areas with a great diversity of plant and animal species, essential for the cycling of nutrients and oxygen and, therefore, for humans.

This research focuses on studying the action of biomass burning aerosols in an area of semi-deciduous forest located in the southern portion of the Amazon Basin, in the north of the State of Mato Grosso, in the region of the arc of deforestation, contributing to a better understanding of the cycle of carbon in the region. To this end, we specifically seek to: (1) develop a clear-sky irradiance algorithm using a long observation period of AOD_a; (2) quantify the increase in the diffuse fraction of solar radiation at the expense of the presence of aerosols from fires in the experimental study area; (3) quantify net and relative changes in carbon fluxes through net ecosystem productivity ($NEE\ of$ CO_2); (4) to evaluate the influence of fires on biophysical variables that influence forest photosynthetic rates (Td_f, T_{air} and Vapour-Pressure Deficit). Aerosol data and micrometeorological measurements in combination with carbon fluxes measured by the eddy covariance system are used in the period 2005-2009. All solar radiation measurements are evaluated in terms of aerosol data (AOD_a), solar zenith angle (SZA), and relative irradiance f.

2 Data and Methods

2.1 Site descriptions

An area of transitional (semi-deciduous) tropical forest located in the south of the Amazon basin, 50 km northeast of Sinop, in the municipality of Cláudia (Lat 11° 24.75' S, Long. 55° 19.50' W), in the State of Mato Grosso (Figure 1). This forest is located in the arc of deforestation, a region of continuous agricultural expansion, logging, and fires; (Nepstad et al., 2014; Balch et al., 2015; Alencar et al., 2022) (Figures S1, S2, and S3).

Previous studies report the peculiar characteristics of this type of forest; trees with lower height, biomass, and floristic diversity compared to humid tropical forests (Murphy & Lugo, 1986; Nogueira et al., 2008) due to their well-defined seasonal period (dry and rainy). The forest is 423 m above sea level, in a transition where the vegetation consists of savannah (cerrado), transitional vegetation (cerradão), and Amazonian forest, with some parts to the south of the Amazon Basin, near Sinop, recognized as dry forest or semideciduous (Ackerly et al., 1989; Ratter et al., 1978).

The deciduous and semi-deciduous forests within the Cerrado domain, initially covered over 49.95 km^2 in the state of Mato Grosso, but currently 20.50 km^2 of this area is deforested ($\approx 41\%$), and only 14% is located within protected areas (Alencar et al., 2022). The geographic positions of these forests are discontinuous, due to climatic fluctuations that have occurred in the last 10,000 years (Prado & Gibbs, 1993). The tree species at this location are typical of the semi-deciduous forest of the Amazon, with maximum canopy heights varying between 25-28 m. Comprehensive description of the species reported in the region was reported by Ackerly et al. (1989), Lorenzi (2000) and Lorenzi (2002). The soils are acidic with a pH measuring 4.2 and sandy (94% sand), well-drained quartzarenic neosols, poor in nutrients, and with low organic matter (Vourlitis et al., 2001; Oliveira-Filho AT & Oliveira, 2002), with a dry season that extends from May to September (Vourlitis et al., 2002).

The 30-year average annual temperature in this area is 24 °C, with precipitation of approximately 2000 mm/year (Vourlitis et al., 2002). Among the active atmospheric systems are the Bolivian High (BH), South Atlantic Convergence Zone (SACZ), and frontal Systems. To the north, the region is influenced by systems that operate in the Amazon, and the southern portion is affected by extratropical systems, such as frontal systems (Amorim Neto et al., 2015; Saraiva et al., 2016). The loss of leaves (deciduousness) during the dry season (July-September) is quite sensitive to water availability and temperatures (maximum and minimum) in the region. With the arrival of the rainy season (November-

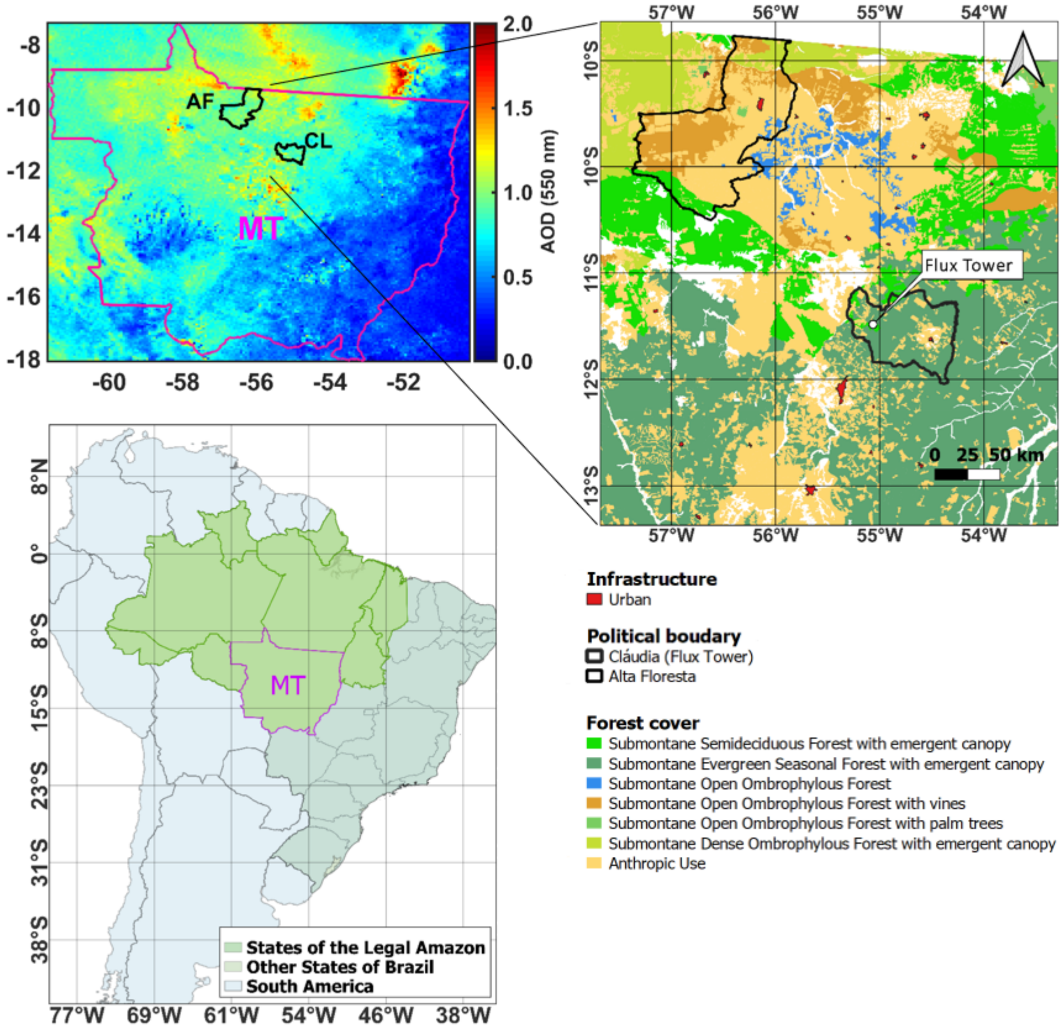

Figure 1. Localization map of micrometeorological tower in the Cláudia municipality, 50 km northeast of Sinop, Mato Grosso (white point, in the right pane).

May), the vegetation recovers again with typical characteristics of tropical forests (Vourlitis et al., 2011).

2.2 Instrumentation and Data

2.2.1 Aerosol Measurements

This study used a long series of aerosol optical depth measurements - AOD (Aerosol Optical Depth) to assess the impact of atmospheric particles on the flux of solar radiation to the surface. Two types of remote sensors were used: the MODIS (Moderate Resolution Imaging Spectroradiometer) orbital sensor, available on board the AQUA and TERRA satellites, products MOD04-3K and MYD04-3K (Remer et al., 2013); and an AERONET (Aerosol Robotic Network) solar photometer, used as a standard measure of optical properties of atmospheric aerosols at the surface, between June1993-March2018 (Holben et al., 1998). All remote aerosol information required for this study was operated and maintained by NASA (National Aeronautics and Space Administration).

The TERRA /AQUA satellites have a heliosynchronous polar orbit with a Local Time (LT) of passage over the study areas around 10h30min and 13h30min. These space platforms cover the Earth's surface every 1-2 days with radiance measurements in 36 spectral bands. The MOD/MYD043K aerosol products also feature the most current collection of data available from NASA, currently at 3 Km spatial resolution for AOD and other aerosol optical properties (Levy et al., 2013; Remer et al., 2013). Filters to exclude contamination of data by clouds are also applied during estimation processing. The AOD series from these satellites has 20 years of data on continents and oceans and is widely available on the open access platform of the Atmospheric Files Distribution System - Level 1, located at the Distributed Active Files Center (LAADS-DAAC) from Goddard Space Flight Center - GSFC, in Greenbelt, Maryland (USA). In this work, satellite AOD spatializations were used to obtain regional information on the nature or type of aerosol acting over the study area, between 2002-2020 (Figure S4). More detailed information about the MODIS sensor, such as spectral models, validation, and operating period of the aforementioned products can be found in (Remer et al., 2005, 2013).

Regarding seasonal forests in northern Mato Grosso, in Alta Floresta, a long series of AOD measurements ($>$ 20 years of data) are available through CIMEL Electronique solar photometers, maintained and operated by NASA (GSFC), through the AERONET network (1993-2021). This photometer network is intended for the monitoring and characterization of aerosol particles in various regions of the world. These sensors represent the standard measure of AOD and are widely used in the validation of satellite AOD estimates. The system operates solar radiation measurements and rotational interference filters to extract optical properties from aerosols in various spectral bands, between 340-1020 nm (Schafer, Holben, et al., 2002; Schafer, Eck, et al., 2002; Procopio et al., 2004; Schafer et al., 2008). This makes it possible to evaluate the direct influence of atmospheric particles in real time on regions highly affected by fires, such as the region of the arc of deforestation. In this work, AOD was used at wavelengths of 500 nm (AERONET) and 550 nm (MODIS). Both satellite and photometer data cover the entire period of micrometeorological and flux data, described in the next section. In the Alta Floresta, the AERONET system also has individual sensors and long-term measurements of incident shortwave solar radiation (SW_{ia}), as described in Table 1.

2.2.2 Micrometeorological Measurements

The CO_2 flux data set available for this research were widely used and cited by previous studies. Information regarding the systems installed in the micrometeorological tower is directly available in (Vourlitis et al., 2011). An automatic weather station (ASW) to monitor the weather in the Cláudia municipality was used between Jun2005 and Jul2008. The implanted tower follows the standard of the micrometeorological measurement tower system of the Programa LBA (L. Nagy et al., 2016; Artaxo et al., 2022). In this research, the deployed tower consists of a pyranometer, thermometer, psychrometer, anemometer, pluviograph, and a turbulent vortex system (*eddy covariance*). Herein, these measures were used to represent the biophysical factors that affect the photosynthetic rates of forests. Micrometeorological data were measured every 30-60 s and stored by datalogger systems (CR5000) and (CR-10X), both Campbell Scientific, Inc., from which hourly averages were calculated (Vourlitis et al., 2011). The micrometeorological data set used in this work is the same used in the study prepared by Vourlitis et al. (2011), whose data are previously validated (certified). Technical details such as precision, accuracy, and calibration can be found in (Vourlitis et al., 2011; Moreira et al., 2017). All direct measurements used are listed in Table 1.

2.2.3 Measures of flux and concentration of CO_2

In Amazonia, the eddy covariance system has been widely used to measure the net CO_2 flux by the ecosystem. This system performs measurements by correlation of tur-

Table 1. List of measured variables and instrumentation used in the micrometeorological tower (at Cláudia Municipality) and AERONET station, in Alta Floresta. The *flags* [1], [2] and [3] indicate the instrumentation used in the flux tower, AERONET system and AQUA space platforms (TERRA), respectively.

Data set	**Instrumentation**		**Attributes**		
Measurements	**Sensors [sites]**	**Models, Manuf.**	**Units**	**Symbols**	**Height**
Inc. Solar Radiation	Pyranometer [1]	LI-200SB, LI-COR	Wm^{-2}	SW_i	40.0 m
Photosyn. Active Rad.	Pyranometer [1]	LI-190SB, LI-COR	Wm^{-2}	PAR_i	41.5 m
Atmospheric Pressure	Barometer [1]	PTB101B, VSLA	hPa	P_{air}	42.5 m
Air Temperature	Thermohygrometer [1]	CS215, RMS	°C	T_{air}	41.5 m
Relative Humidity	Thermohygrometer [1]	HMP-35, VSLA	%	RH_{air}	41.5 m
Precipitation	Pluviometer [1]	GAUGE, MANUAL	mm	PRP	40.5 m
Wind Speed	Sonic Anemometer [1]	CSAT-3, CSCI	ms^{-1}	US_s	42.0 m
Wind Direction	Sonic Anemometer [1]	CSAT-3, CSCI	deg	US_d	42.0 m
CO_2 Concentration	IRGA [1]	LI-820, LI-COR	ppm	$[CO_2]$	1-28 m
Inc. Solar Radiation	Pyranometer [2]	CM21, K&Z	Wm^{-2}	SW_{ia}	–
Photosyn. Active Rad.	PAR Energy [2]	SKYE510, SKYE	Wm^{-2}	PAR_{ia}	–
Aerosol Optical Depth	Photometer [2]	CIMEL	-	AOD_a	–
Aerosol Optical Depth	Modis-Terra [3]	MOD043K	-	AOD_m	–
Aerosol Optical Depth	Modis-Aqua [3]	MYD043K	-	AOD_m	–

bulent vortices from a sonic anemometer and an infrared gas chamber (Infrared Gas Analyzer, IRGA), from which flux measurements of CO_2 (Carbon), water vapor (H_2O) and energy (sensible heat – H and latent heat – LE) are determined at high frequency, usually 10Hz. The data generated and recorded by the *eddy* system, deployed in flux towers, is normally adjusted by compilation software such as Alteddy 3.90 (Alterra, WUR, Netherlands), from which averages are taken every 10, 30 or 60 min (Foken, 2008). This system has been extensively described and improved in recent years (Moncrieff et al., 1997; Aubinet et al., 2001; Aubinet, 2012). The carbon flux data from these micrometeorological towers are presented, using the classical sign convention in atmospheric science. The negative flux, by convention, indicates that the displacement of the net flux of CO_2 is downward (photosynthesis), that is, the vegetation or ecosystem is absorbing carbon, while the positive flux is characterized by the release of carbon (respiration). (Goulden et al., 2004). The flux of CO_2, in particular, is a critical variable in the calculation and determination of the net exchange of CO_2 at the interface of any ecosystem, without which it is not possible to calculate the NEE *of* CO_2, according to the analysis methods described in the sections below. This procedure is possible through the coupling between LI-COR and eddy covariance systems, as illustrated in Vourlitis et al. (2002) and Vourlitis et al. (2011).

2.3 Methods

This section describes the methodological procedures used to achieve the radiative effects of aerosols on the NEE of CO_2 presented in section 1.1. Initially, the technical procedures used to determine the net exchange of CO_2 and to obtain the clear sky irradiance model, a critical step in the calculation of the relative irradiance, are presented. Next, the procedures for calculating diffuse PAR radiation and relative change NEE ($\%NEE$), used to assess ecosystem responses to fire pollution loads, are described. Procedures to assess the influence of environmental factors on NEE due to fires are also described.

2.3.1 Method to determine the net exchange of CO_2 in the ecosystem

The NEE is obtained from turbulent flux measurements using the eddy covariance technique taking into account the storage term S[CO_2] (Aubinet, 2012; Araújo et al., 2010). Micrometeorological sensors distributed vertically along the tower are essential for the NEE calculations (Hollinger & Richardson, 2005), using continuous measurements of the CO_2 profile between soil and the top of the tower. Under these conditions, NEE can be approximated by Equation 1:

$$NEE \approx FCO_2 + S[CO_2]_p \tag{1}$$

where FCO_2 is called "CO_2 turbulent flux", calculated by the *eddy* system, above the treetops (Grace et al., 1996; Burba, 2013); $S[CO_2]_p$ is the vertical profile of the concentration of CO_2 or storage term (storage), considered a non-turbulent term, measured at discrete levels z, at thicknesses Δz_i, from near the ground surface to the point of measurement of covariance of turbulent vortices in the tower (Finnigan, 2006; Araújo et al., 2010; Montagnani et al., 2018). In this work, the vertical profile $S[CO_2]_p$ was stratified into 5 reference levels (1, 4, 12, 20, and 28 m). Typical diurnal conditions consist of vector winds with speeds of 2.0 ms^{-1} and $u^\star$ = 0.20 ms^{-1} and predominant SSW and SE directions. Approximately 72% of the accumulated flux originates within 1 km and the representativeness of the measured CO_2 flux (footprint) is approximately 520 m (upstream of the tower), following the model proposed by (Schuepp et al., 1990). The concentrations [CO_2] were calculated following Aubinet et al. (2001) and Araújo et al. (2010), as reported by Vourlitis et al. (2011).

$$S[CO_2]p = \frac{\mathrm{P}_{air}}{\mathrm{RT}_{air}} \int_0^z \frac{\partial[\mathrm{CO}_2]}{\partial t}\, dz \tag{2}$$

Where: P_{air} is the atmospheric pressure (Nm^{-2}), R is the molar constant of the gas ($\mathrm{Nm\ mol}^{-1}\ \mathrm{K}^{-1}$) and T_{air} the air temperature in (°C).

2.3.2 Method to determine the solar irradiance of clear sky

The term clear sky was used here to designate the minimal influence of clouds and aerosols on the the solar radiation measured by the pyranometer. To estimate the amounts of direct solar radiation to the surface under minimally overcast sky conditions, the measurements SW_{ia} of the AERONET 2.0 system (*cloudless*) observed under clear-sky conditions were used, that is, AOD $\leq$ 0.10 (Artaxo et al., 2022), in the absence of fire plumes. Under these conditions, we get the Equation 3; a polynomial fit of order 4, here, considered representative of the entire solar spectrum (Meyers & Dale, 1983). The model $S(t)_0$ obtained was used to derive the clear-sky instants at the surface (Figure S4), between 07-17h (LT), according to the formulation below:

$$\mathrm{SW}_{ia}\{\mathrm{AOD} \leq 0.10, \mathrm{cloudless}\} \approx S(t)_0 = at^4 + bt^3 + ct^2 + dt + e \tag{3}$$

Where $S(t)_0$ is the clear-sky solar irradiance as a function of time, in Wm^{-2}. The parameters (a, b, c, d, e) are the coefficients of the polynomial curve and t, the time, in local hours (LT). Figure 2 shows the mean diurnal cycle of the SW_{ia} in the tower observation area under different pollution conditions. The plot illustrates the sensitivity of the method applied to determine the expected irradiance levels on the canopy forest ($S(t)_0$) under varied atmospheric aerosol loads (AOD), C2, C4, and C6 curves.

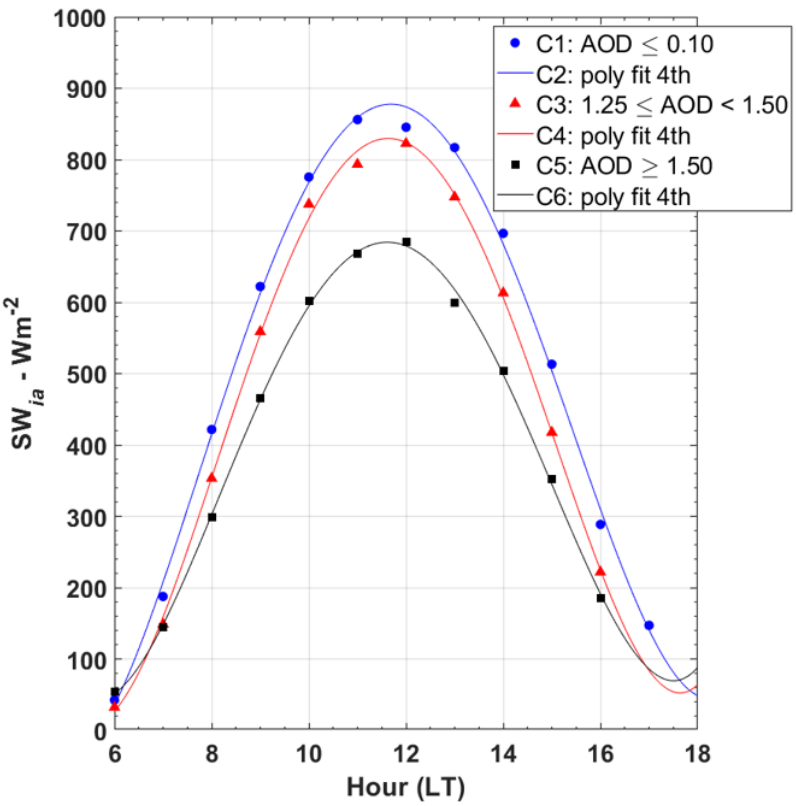

Figure 2. Incident solar irradiance under different sky conditions in Alta Floresta (1993 to 2018): clear-sky (C2 curve, AOD $\leq$ 0.10) and polluted-sky (C4 curves) and C6, AOD $\geq$ 1.25).

Using the long series of measurements of AOD$_a$ it was possible to obtain different curves $S(t)_0$ for each month of the year, taking into account the seasonal variations of the SW$_{ia}$ given in Equation 3. Figure S4 shows the seasonal variation of the $S(t)_0$ diurnal cycle throughout the year. The coefficients of the fit curves it listed in Table S1. To assess the consistency of the $S(t)_0$ model, obtained by SWia AERONET data set, we compared the outputs calculated by Equation 3 with the clear-skies solar irradiance model available by the Meteoexploration (SolarCalculator).

2.3.3 Determination of relative irradiance

In practical terms, the relative irradiance f expresses the relationship between incident solar radiation and that observed at the surface under a clear sky (AOD $<$ 0.10) and “free” of clouds ($f > 1.0$). To determine it, it is necessary to calculate $S(t)_0$, given in the previous section. It is a parameter indicating the presence of clouds and/or pollution plumes with aerosols that scatter solar radiation, generally used in areas without direct instrumentation of cloud cover over the flux tower observation area. In these cases, f is considered a key indicator in the detection of clouds and plumes of pollution from fires in the Amazon. For this, the observed amounts of SW$_{ia}$ on the forest canopy were normalized by the irradiance $S(t)_0$; both variables in Wm^{-2}, thus determining the quotient f (dimensionless parameter), according to Equation 4 below.

$$f = \frac{\mathrm{SW}_{ia}\{\mathrm{AOD_a} > 0.10, \mathrm{cloudness}\}}{S_0\{\mathrm{AOD_a} \leq 0.10, \mathrm{cloudless}\}} \tag{4}$$

Where: SW_{ia} is the total incident solar irradiance measured by the pyranometer ($\mathrm{Wm^{-2}}$) under any atmosphere ($\mathrm{AOD}_a > 0.10$) and in the possibility of clouds (*cloudness*) and $S(t)_0$ is the clear sky solar irradiance ($\mathrm{Wm^{-2}}$) on a flat surface perpendicular to the sun's rays, without the attenuating effects of the atmosphere (clouds and burned) for a given time and place, ie $\mathrm{AOD}_a \leq 0.10$ (*cloudless*). Values off close to zero represent cloudy and/or smoky-sky conditions, and values close to unity represent clear-sky conditions (Gu et al., 1999; Oliveira et al., 2007; Jing et al., 2010; G. G. Cirino et al., 2014; Gao, 2020).

Here, we used f as a basis for comparison to detect the joint presence of clouds and aerosols from fires over the study area, since the experimental site does not have instrumentation for direct observation of cloud cover. Obtaining this parameter is extremely important because when using clear-sky solar radiation as a base, solar radiation measured under overcast skies becomes a new metric for observing cloudiness. This variable will be compared with the NEE to assess the photosynthetic responses of the ecosystem to variations in the external environment.

2.3.4 Determining the clarity index

To determine the parameter kt (here defined as brightness index) the extraterrestrial solar irradiance S_{ext} was first calculated (depending only on orbital parameters). The index kt is a coefficient of proportionality between the measurements of direct solar radiation to the surface and S_{ext}. This index expresses the direct solar radiation transmitted in the atmosphere (Gu et al., 1999; G. G. Cirino et al., 2014). In a first approximation kt indicates the transmissivity; the degree of transparency of the atmosphere to solar radiation at a given time and place, while f is a parameter of comparison more sensitive to the presence of radiation-scattering aerosols and clouds. Here, kt and SZA were used as predictors of the diffuse component of (Gu et al., 1999; G. G. Cirino et al., 2014) radiation. For the calculation of the irradiance S_{ext} some parameters and variables are also needed such as the solar constant of the Earth (S^t_{ext}), the latitude of the location (φ), solar declination (δ), hour angle (h) and mean square distance between the Earth and the Sun (Gates, 1980). The determination of S_{ext} takes into account the angle of incidence of the solar rays and, therefore, the variations in the amounts of solar radiation at the surface, modulated by the SZA. Under these conditions, kt can be expressed according to Equation 5:

$$kt = \frac{\mathrm{SW}_i\,\{AOD > 0.10, cloudiness\}}{S_{ext}} \tag{5}$$

Where SW_i is the short wave radiation measured by the pyranometer ($\mathrm{Wm^{-2}}$) (Table 1) and S_{ext} the extraterrestrial solar irradiance ($\mathrm{Wm^{-2}}$) estimated on a perpendicular surface to the sun's rays, without the attenuating effects of the atmosphere for a given time and place, expressed according to 6.

$$S_{ext} = S^t_{ext}\left(\frac{\bar{D}}{D}\right)^2 \times cos(z) \tag{6}$$

In this equation S^t_{ext} is the Earth's solar constant ($\approx 1367\ \mathrm{Wm^{-2}}$), $\bar{D}$ is the average Earth-Sun distance ($\sim 1.49 \times 10^6$ km), D is the Earth-Sun distance on a given Julian day, and cos (z) the cosine of the solar zenith angle (SZA), calculated as proposed by Bai et al. (2012). This calculated index was used to establish the diffuse solar radiation, as described in detail in the next section.

2.3.5 Determination of diffuse PAR radiation

To determine the diffuse component of the total PAR (PAR_d), we adopted the procedures of (Spitters et al., 1986) and (Reindl et al., 1990), widely used in the literature when there are no direct measurements of radiation PAR_d (Gu et al., 1999; Jing et al., 2010; Zhang et al., 2010; Bai et al., 2012). The detailed calculation can be found in the one performed by Gu et al. (1999). The estimate is performed by deriving the diffuse PAR radiation according to the formulation below (Spitters, 1986).

$$PAR_d = \left[\frac{1 + 0.3\left(1 - q^2\right) q}{1 + (1 - q^2)\cos^2(90 - z)\cos^3(z)} \right] \times \mathrm{PAR}_i \tag{7}$$

Where PAR_d is the incidence of the diffuse (total) PAR radiation flux (μmol photon m^{-2}s^{-1}), in the near-infrared range, in a horizontal plane to the Earth's surface, while q is a coefficient of proportionality used to denote the ratio of the total diffuse radiation to a given amount of irradiance (SW_i) at the surface, under a given condition of the sky (Wm^{-2}). The parameter q is expressed considering ranges of variation for the index kt (Gu et al., 1999). To express the diffuse fraction of PAR radiation ($PAR(D)_f$) we use the relationship between PAR_d and PAR_i (Spitters et al., 1986). In the absence of direct measurements of diffuse solar radiation, the procedures reported by these authors are still widely used (Jing et al., 2010; G. G. Cirino et al., 2014; Moreira et al., 2017).

2.3.6 Determining the efficiency of light use

Another important parameter in this kind of study is the light use efficiency (LUE), which expresses the efficiency of light use in photosynthetic processes by the canopy. It is defined as the ratio between NEE and PAR_i. Several other procedures have been used to approximate the LUE, some use the coefficient of proportionality between the NEE and the PAR_d (Moreira et al., 2017) radiation, and others use temperature measurement directly on the leaf of the trees (LI-COR) to capture the photosynthetic response as a function of the variation in light intensity (Doughty et al., 2010). Canopy radiative transfer codes with validated physical parameterizations for different leaf types are also used (Mercado et al., 2009). Here, for practical reasons, we used the procedures applied by Jing et al. (2010) and G. G. Cirino et al. (2014), according to Equation 8, where LUE is given in percentage values.

$$LUE \approx \left(\frac{NEE}{\mathrm{PAR}_i} \right) \tag{8}$$

2.3.7 Determining leaf canopy temperature

The model used to estimate the Td_f was obtained from field experiments in central Amazonia, at sites T14, T34, TN-S, and BBL4, approximately 60-70 km NW from the center of Manaus-AM. Micrometeorological and temperature measurements with thermocouples on leaves were performed on 25 and 22 samples for two different types of healthy plant species, typical of central Amazonia, distributed between 18-35 meters above the ground during the dry (July-August/2003) and rainy seasons (December 2003-February 2004), respectively. Leaf temperature measurements were performed every 15 min, between 07h and 14h (LT). Doughthy et al. (2010) used alternative procedures based on pyrometer measurements to estimate leaf canopy temperature in the Tapajós National Forest (FLONA-Tapajós), in Santarém-PA, obtaining similar Td_f diurnal cycles. Here, in the absence of direct leaf temperature measurements or data from pyrgeometers operated above the canopy to measure the emission of long-wave radiation from the LW_c surface in the experimental tower (Table 1), we estimate the leaf canopy temperature (Td_f) through the formulation proposed by Tribuzy (2005). The final equation obtained is expressed as a function of relative air humidity (RH_{air}) and PAR_i radiation, as shown below:

$$Td_f = [(2.48 \cdot 10^{-6}(\mathrm{RH}_{air})^2 - 1.82 \cdot 10^{-4}(\mathrm{RH}_{air}) - 1.83 \cdot 10^{-6}(\mathrm{PAR}_i) + 0.0363)]^{-1} \quad (9)$$

2.3.8 Determination of clear sky NEE

The NEE observed on clear days (AOD < 0.1 and clear) was also used as a basis for comparison for cloudy days and/or days with high aerosol loading. The Figure 3 illustrates the behavior of the NEE under clear sky conditions ($f \approx 1.0$). The polynomial fit obtained is used to determine the clear sky $NEE(sza)_0$ as a function of SZA variations, between Jun2005-Jul2008. Figure 3 below illustrates the NEE variations as a function of the SZA angle. The correlation curve found is consistent with the behavior observed in previous studies (Gu et al., 1999; G. G. Cirino et al., 2014). The equation below was used to estimate the expected NEE under the above-mentioned conditions.

$$NEE(sza)_0 = p_1t^2 + p_2t + p_3 \quad (10)$$

Where $NEE(sza)_0$ is the NEE typically found on clear sky days (μmol $\mathrm{m}^{-2}\mathrm{s}^{-1}$). The parameters p_1, p_2 and p_3 the coefficients of the polynomial curve obtained, respectively equal to: 0.0038, $-$ 0.99 and $-$ 12. Like f, $\%NEE$ was used here as a basis for comparison for the maximum negative values observed between Jun2005-Jul2008, assuming, in this analysis, the absence of water stress and nutrient deficiency in the studied period (Gu et al., 1999; Oliveira et al., 2007; Doughty et al., 2010; G. G. Cirino et al., 2014).

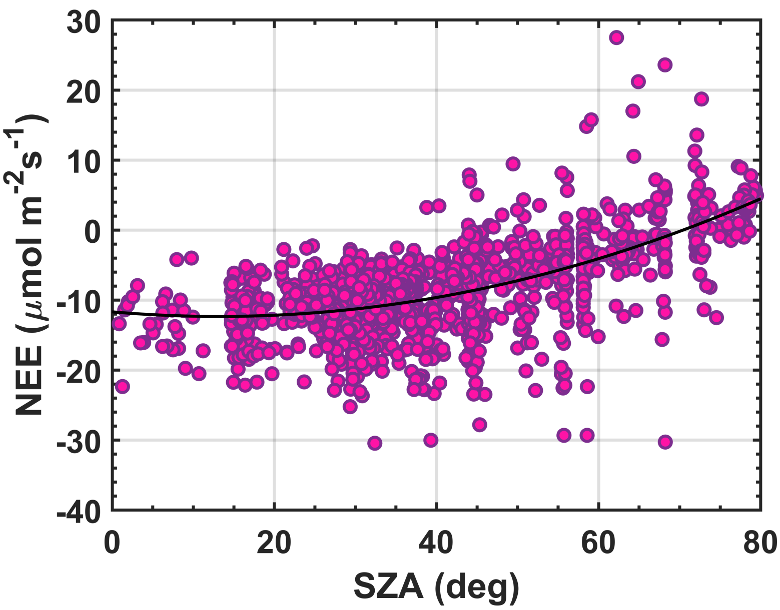

Figure 3. Correlation between NEE and SZA for clear sky conditions ($f \approx 1.0$), in the Cláudia Municipality. The black curve indicates the 2nd order polynomial fit obtained ($NEE(sza)_0$).

Changes in observed NEE versus NEE under clear sky conditions were used to determine the percentage effect of aerosols on NEE. The $\%NEE$ was calculated by the following relationship (Bai et al., 2012; Gu et al., 1999; Oliveira et al., 2007):

$$\%NEE = \left(\frac{NEE(sza) - NEE(sza)_0}{NEE(sza)_0} \right) \times 100 \tag{11}$$

To largely eliminate solar elevation angle interference in the analysis of changes in $\%NEE$ versus f, we grouped the data into SZA ranges of 20-25°. This interval was small enough to minimize the effects of solar uplift during the day and to represent changes in NEE as a function of f in response to changes in NEE flux due to aerosols and/or clouds alone. This interval also ensured sufficient sample size for statistical analyses. SZA intervals smaller than 15° significantly reduced the sample size, making it impossible to develop a robust statistical analysis (Gu et al., 1999). Values above 50 or around 0 (solar angles very close to the horizontal and vertical plane, respectively) were, in general, very contaminated by clouds (Gu et al., 1999; G. G. Cirino et al., 2014).

2.4 Data analysis procedures

Computational routines were developed for compilation, certification, organization, and analysis of the variables presented in Table 1. We performed fitting curves and mathematical or statistical calculations with the packages available in (MATLAB, 2013). For data quality control, non-physical values outside acceptable levels were excluded from the database, totaling a loss of 3% of the total set of valid measurements (approximately 3,600 sampled points). Data analysis consists of three fundamental steps: (1) variation of solar radiation with optical depth AOD_a analyzed as a function of irradiance f; (2) effects of aerosols and clouds on the net exchange of CO_2 at the forest-atmosphere interface and, finally, (3) quantification of photosynthetic performance as a function of pollution loads, from which to extract if the biological critical or optimal values for environmental (exogenous) factors such as d, T_{air}, Td_f and VPD. Photosynthetic performance, in all cases, is analyzed as a function of NEE. In the end, the net percentage variation of the photosynthetic activity of the forest ($\%NEE$) is evaluated as a function of the irradiance f. The main statistical analysis procedures adopted are performed in terms of correlation graphs (3D scatter plots), that is, through the direct correlation between two or three variables simultaneously, from which regression curves are determined and used to compose the representative polynomial equations of the processes under analysis. The relationships found are evaluated from the Poisson correlation and tabulated in terms of basic descriptive statistical parameters such as coefficient of determination (R^2) and significance level (P_{value}) with a margin confidence of 95%. Basic descriptive statistics is also applied to the data to obtain mean values, medians, percentiles, and standard deviation for the measured and estimated variables. Table 2 lists indirect variables, calculated from the dataset listed in Table 1.

3 Results and Discussions

3.1 Average daily cycle of net exchange of CO_2

The average daily pattern of NEE variation follows the typical pattern of tropical forests in the Amazon and other tropical forests (Gu et al., 1999; Niyogi et al., 2004; von Randow et al., 2004; Araújo et al., 2010; Doughty et al., 2010). The maximum negative fluxes average -13.7 ± 6.2 μmol m^{-2}s^{-1}, often observed around 10-11h (LT), and the maximum positive $+6.8 \pm 5.8$ μmol m^{-2}s^{-1}, approximately constant during the night period between 19h and 05h (LT), considering the data for the entire year, between 2005-2008. These results are consistent with the processes of photosynthesis (during the day) and respiration (predominantly nocturnal), respectively. We observed a slight difference

Table 2. List of indirect (calculated) variables, symbols, and measurement units of derived quantities, according to the cited body of literature.

Indirect Measures	**Symbols**	**Units**	**Literature**
CO_2 Net Exchange	NEE	μmol m^{-2}s^{-1}	(Vourlitis et al., 2011)
CO_2 Flux	FCO_2	μmol m^{-2}s^{-1}	(Vourlitis et al., 2011)
CO_2 Vertical Profile	$S[CO_2]_p$	ppm	(Araújo et al., 2010)
Clear Sky Solar Irradiance	$S(t)_0$	Wm^{-2}	(Author)
Solar Zenith Angle	SZA	Degrees	(Bai et al., 2012)
Relative Irradiance	f	-	(G. G. Cirino et al., 2014)
Clarity Index	kt	-	(Gu et al., 1999)
Extraterrestrial Solar Irrad.	S_{ext}	Wm^{-2}	(Gu et al., 1999)
Diffuse PAR Radiation	PAR_d	μmol phot. m^{-2}s^{-1}	(Gu et al., 1999)
Diffuse PAR Fraction	$PAR(D)_f$	-	(Gu et al., 1999)
Efficiency of Light Use	LUE	-	(Jing et al., 2010)
Leaf Canopy Temperature	Td_f	°C	(Tribuzy, 2005)
Clear Sky NEE Exchange	$NEE(sza)_0$	μmol m^{-2}s^{-1}	(G. G. Cirino et al., 2014)
Relative NEE Exchange	$\%NEE$	%	(G. G. Cirino et al., 2014)

in the pattern of the daily cycle of the NEE flux between the wet and dry seasons (Figure (4)), with CO_2 absorption peaks about 10-15% lower (i.e, less negative) at both seasons (< 0.6 μmol m^{-2}s^{-1}), when compared to the results presented by Vourlitis et al.. Our results also show a shift (an advance) in the peak absorption of CO_2 from the wet-to-dry season, from about 12h (LT) to 10h (LT), respectively (Figure 4).

Seasonal variations in water availability, nutrients, radiation, temperature, VPD, and pollution are counterbalanced throughout the year, producing an average seasonal behavior without significant differences in NEE. Vourlitis et al. (2011) showed similar monthly variations with more negative magnitudes during the bright hours of the day in the rainy months (-9.0 μmol m^{-2}s^{-1}, between November-February) and less negative during the light hours in the dry months (-7.7 μmol m^{-2}s^{-1}, between May-August). During night hours these values are respectively equal to $+5.4$ μmol m^{-2}s^{-1} and $+7.4$ μmol m^{-2}s^{-1}. The general balance between these fluxes reveals 'carbon uptake' of -0.12 μmol m^{-2}s^{-1} and -0.18 μmol m^{-2}s^{-1} during the wet and dry seasons, respectively. The maximum rates of photosynthesis and leaf canopy respiration, between 2005-2008, were systematically observed between October-November, usually, in the first months of the rainy season (Vourlitis et al., 2011).

3.2 The influence of aerosols on solar radiation

The impact of aerosol particles by fires on the SW_i flux is evaluated as a function of f, AOD_a, SZA, $PAR(D)_f$ and PAR_i. Figure 5 (top panel) shows the behavior of the relative irradiance f for different levels of AOD_a pollution, in the SZA ranges between 20-50°. A close and statistically significant relationship between f and AOD_a is observed with p-value < 0.01 and R^2 of about 0.92 (Table 3). An approximately linear relationship is observed in which f decreases by about 40-60% when the AOD_a varies from 0.10 to 5.0. No statistically significant difference was observed between mornings and afternoons in these analyses. There is only a slight increase of $\approx$ 5-20% (on average) in the value of f between late mornings and afternoons, attributed here to the multiple scat-

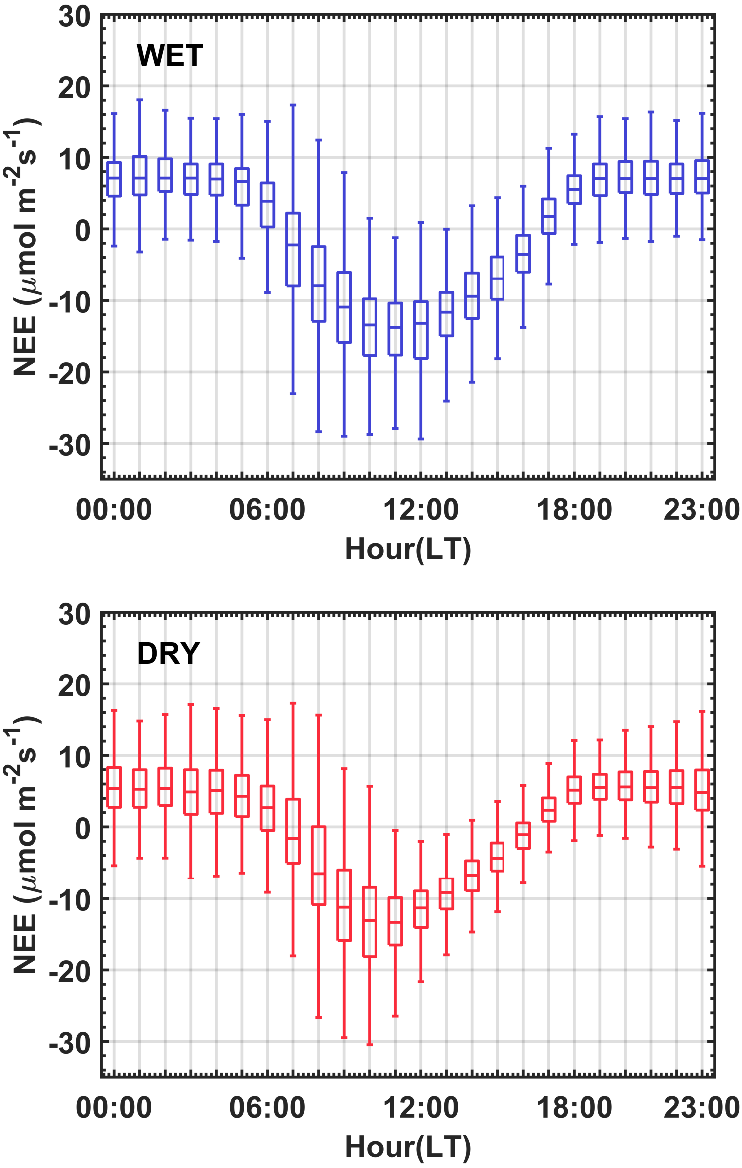

Figure 4. NEE average hourly cycle between June/2005 and July/2008, during the rainy (WET) and less rainy (DRY) seasons in a semideciduous forest in the Cláudia municipality, 50 km northeast of Sinop, Mato Grosso. The standard deviation is shown as vertical bars.

tering of solar radiation due to the formation of clouds nearby from the observation tower (Gu et al., 2001). For SZA angles between 20 and 50°, there is a strong reduction in the amounts of SW$_i$ (225 ± 50 Wm^{-2}) associated mainly with the increase in the concentration of aerosols emitted by local fires or transported regionally during the burning season. Oliveira et al. (2007) and G. G. Cirino et al. (2014) reported results about 2-3 times lower for 20-30% reductions in f and AOD increase from 0.1 to 0.8, in FLONA-Tapajós (Santarém-PA) and central Amazon (K4), in Manaus-AM.

Figure 5 (bottom panel) shows the fraction of diffuse radiation calculated as a function of AOD$_a$, identifying important statistical relationship is also observed ($R^2 = 0.98$ and 0.96) for the morning and afternoon hours (Table 3). Due to the reduction in the instantaneous fluxes of SW_i an increase of about up to 85% in diffuse radiation is observed when the AOD_a increases from 0.10 to 5.0. These results are consistent with previous studies carried out in the Brazilian Amazon (Doughty et al., 2010; G. G. Cirino et al., 2014; Rap, 2015; Moreira et al., 2017; Malavelle et al., 2019; Bian et al., 2021) and also around the world (Niyogi et al., 2004; Jing et al., 2010; Rap, 2015; Rap et al., 2018) and proves to be particularly important due to to the ability of PAR_d to penetrate more efficiently into the leaf canopy contributing, under certain conditions, to a significant increase in carbon uptake by the ecosystem.

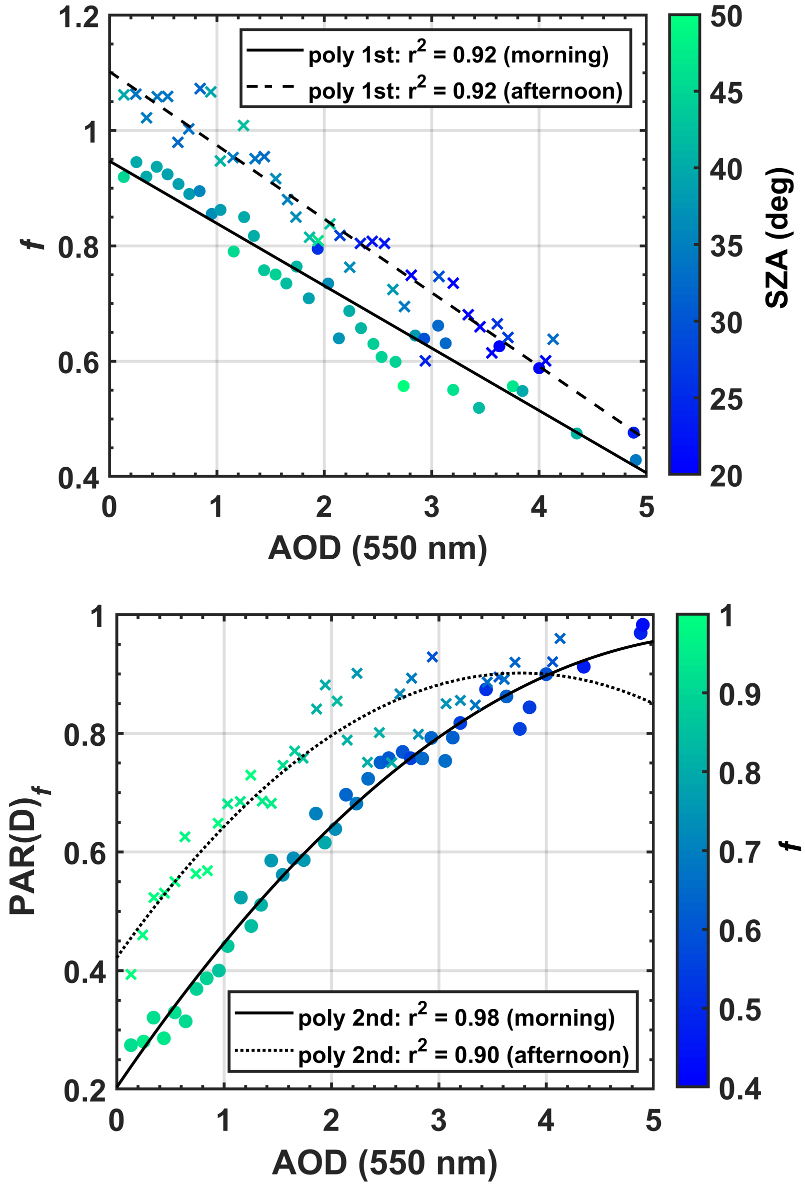

Figure 5. 3D-correlation between f and $PAR(D)_f$ with increasing AOD_a for different values SZA (top panel) and irradiance f (bottom panel) in semi-deciduous forest in the Cláudia municipality, 50 km northeast of Sinop-MT (2005-2008).

Table 3. Polynomial adjustments (Figure 5), coefficients and statistics for the morning and afternoon periods in the micrometeorological tower in Cláudia-MT (2005-2008). R^2 is the correlation coefficient, ΔSW_i is the incident shortwave radiation amount, and STD is the Standard Deviation.

Settings		**Period**	**Coefficients**			**Statistics**	
Polynomial Functions		**Local Hours**	***a***	***b***	***c***	$\mathbf{R^2}$	$\Delta\mathbf{SW}_i$ **(STD)**
f	poly fit 1st	07-12h	-0.11	0.95		0.92	-200 ($\pm$ 50)
		12-17h	-0.13	1.10		0.92	-250 ($\pm$ 80)
$PAR(D)_f$	poly fit 2nd	07-12h	-0.023	0.27	0.20	0.98	-97 ($\pm$ 30)
		12-17h	-0.034	0.25	0.42	0.90	-118 ($\pm$ 42)

3.3 The influence of aerosols on PAR radiation

Figure 6 shows the behavior of the radiation PAR_i and PAR_d as a function of f and SZA. For reductions of $\approx$ 40% in f, that is, for f ranging from 1.0 to 0.6, strong reductions in radiation PAR_i ($\sim$ 750 μ mol $m^{-2}s^{-1}$), corresponding to a 55% increase in radiation PAR_d ($\sim$ 600 μmol $m^{-2}s^{-1}$). This behavior was observed between July-November of the years 2005-2008, during selected clear-sky days. These numbers indicate a strong reduction in PAR_i as pollution levels increase and change from clear sky conditions (AOD $\leq$ 0.10, $f \sim 1.0$) to aerosol smoky sky conditions of fires (AOD $\gg$ 0.1, $f \ll 1.0$).

PAR_i decreased almost linearly with respect to f (Figure 6, top panel). The relationship between PAR_d radiation and f does not show a linear behavior (Figure 6, bottom panel). PAR_d values reach maximum values (779-1080 μmol $m^{-2}s^{-1}$) for values of f between 0.63 and 0.66 (reductions of 37 %-34%) for ranges SZA (20-40°). As will be seen below, these values are considered critical for maximum CO_2 absorption rates (maximum-negative NEE). The 50% increase in PAR_d can be explained by aerosol dispersion during the biomass burning season (July-November), results mainly attributed to the dense layer of radiation-scattering aerosols, typical of Biomass Burning Organic Aerosols (BBOA) aerosols (Shilling et al., 2018; de Sá et al., 2019). The polynomial fits, coefficients, and inflection points are displayed in Table 4.

Table 4. Polynomial adjustments (Figure 6), coefficients, and statistics for the morning and afternoon periods in the micrometeorological tower in Cláudia-MT (2005-2008). **C**p (x_v, y_v) is the critical point of the fit curve, where the derivative is equal to zero.

Settings		**Angles**	**Coefficients**				**Etatistic**	
Polynomial Functions		**SZA**	***a***	***b***	***c***	***d***	$\mathbf{R^2}$	**C**p (x_v, y_v)
PAR_i	poly 1st	0-20°	$+1.5\times10^3$	$+56$			0.92	
		20-40°	$+2.0\times10^3$	$+41$			0.86	
		40-60°	$+1.7\times10^3$	$+57$			0.64	
		0-60°	$+1.3\times10^3$	-23			0.67	
PAR_d	poly 3rd	0-20°	-2.5×10^3	$+8.4\times10^2$	$+2.2\times10^3$	-19	0.92	(0.66, 1080)
		20-40°	-1.3×10^3	-5.6×10^2	$+2.3\times10^3$	-56	0.66	(0.63, 846)
		40-60°	-6.4×10^2	-7.0×10^2	$+1.6\times10^3$	-41	0.42	(0.61, 529)
		0-60°	-2.0×10^3	$+5.8\times10^2$	$+1.7\times10^3$	-22	0.40	(0.63, 779)

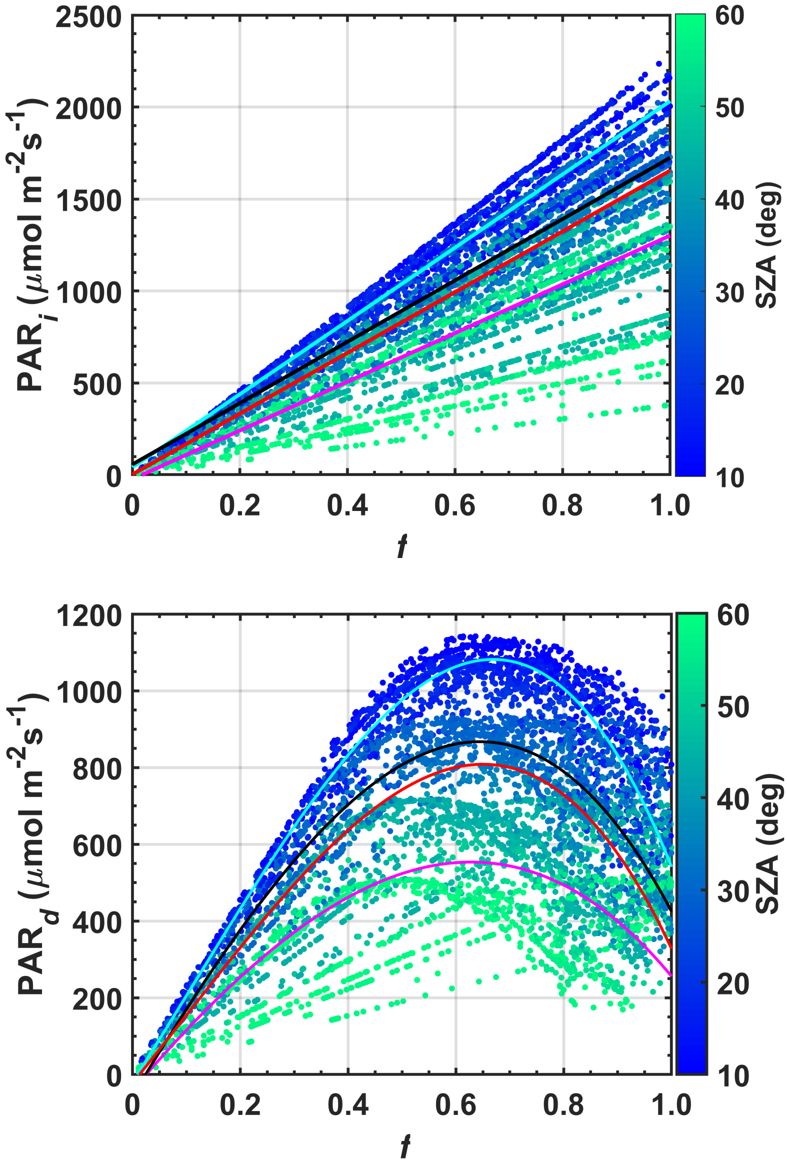

Figure 6. 3D-correlation between f, PAR$_i$ (top panel) and PAR_d (bottom panel) for different SZA values. The blue, black, magenta and red lines are the polynomial curves adjusted to the analyzed SZA variation ranges, respectively equal to 0-20º, 20-40°, 40-60°, and 0-60º, in semi-deciduous forest in the Cláudia municipality, 50 km northeast of Sinop-MT (2005-2008).

3.4 The indirect effect of aerosols on the use of light efficiency by the forest

Due to the burning season, there was a well-defined monthly variation of AOD$_a$, as shown in the previous sections. Since fires are the main cause of changes in the physical and chemical composition of the atmosphere throughout the year (Martin, Andreae, Artaxo, et al., 2010; Martin, Andreae, Althausen, et al., 2010; Artaxo et al., 2013, 2022), statistically significant reductions were found for the SWi flux and radiation PAR$_i$. This section mainly evaluates the optimal levels of PAR$_i$ radiation, as well as the effects of changes in the efficiency of solar radiation use by the forest (LUE). The LUE, here, is expressed in terms of the quotient between the fluxes NEE and PAR_i, Equation 8, as already mentioned in the section before (Sec. 2.3.5). The analyses are performed as a function of PAR_d radiation, from which the maximum efficiency of light use for the studied semideciduous forest is determined.

Under smoky sky conditions (AOD $\gg$ 0.10), carbon assimilation gradually increases with increasing total PAR radiation (PAR_i) reaching maximum saturation around 1550 and 1870 μmol m $^{-2}$s^{-1} in the range between 20-50° SZA, values for which the maximum NEE (negative) occurs around -23 μ mol m^{-2}s^{-1}. Under clear sky conditions, considering the same SZA range, the maximum saturation (maximum negative NEE), occurs around 2100-2300 μmol m^{-2}s^{-1}, that is, around -18 μmol m^{-2}s^{-1} (Figure 7, top panel). To complement this analysis, the NEE flux was normalized by the radiation PAR_i and plotted against the $PAR(D)_f$ during days with high aerosol loading in the burning season (Figure 7, bottom panel). Under these conditions, it is observed that the forest reaches maximum NEE fluxes (negative) on smoky days and not under clear sky (sunny) conditions. The results reveal that smaller amounts of energy are needed for the forest to reach maximum saturation on non-polluted days. The analyzes presented in Figure 7 confirm greater photosynthetic efficiency (under smoky sky conditions) for the studied semideciduous forest ecosystem, results compatible with field observations (Oliveira et al., 2007; Doughty et al., 2010; G. G. Cirino et al., 2014) and by numerical modeling in the Amazon (Rap, 2015; Moreira et al., 2017; Malavelle et al., 2019; Bian et al., 2021) and in the world (Rap et al., 2018). Due to the physicochemical nature of the BBOA and its intrinsic properties (G. Cirino et al., 2018; Adachi et al., 2020) the radiation PAR_d can strongly affect the NEE and the functioning of several other Amazon forest ecosystems (Rap, 2015; Rap et al., 2018; Bian et al., 2021), especially where tree species adapted to low light conditions occur, for example, in the leaf sub-canopy of Amazonian forests (Mercado et al., 2009).

Photosynthetic efficiency (LUE), closely linked to the canopy's ability to convert solar energy into biomass, is $\sim$ 1-2% for the studied forest, indicating loss or rejection of a large part of the solar energy available for photosynthesis. However, for high values of PAR_d, close to 1.0, peaks of up to 3% in photosynthetic efficiency are observed. In situations where the diffuse fraction total maximum values, the values of AOD_a are on average greater than 1.0 and $f \ll 1.0$. These findings corroborate the previous analyzes and reinforce the presence of radiation-scattering aerosols emitted by the fires over the studied area. Although there is great uncertainty (high standard deviation) in the behavior of LUE with increasing radiation PAR_d, there is a gradual, approximately linear increase in the values of LUE in the range of radiation PAR_d between 0.20-1.0. This behavior is peculiar to tall vegetation with a generally leafy canopy of tropical forests, which are more sensitive to the transfer of PAR_d radiation from the top canopy to the bole. In short stature vegetation, as in the semiarid region of northeast China (eg grasses), the LUE remains approximately constant even for high values of PAR_d generated by aerosols and clouds (Jing et al., 2010). Overall, however, the LUE is low for many vegetation types, typically between 1-3%.

3.5 The net absorption of CO_2 due to aerosols from fires

The Equation 11 and Equation 4 allowed us to evaluate the behavior of the ratio between the $\%NEE$ and the irradiance f for intervals SZA from 0-75°. This procedure was adopted to minimize the effects of solar elevation and air temperature on the NEE flux throughout the day (Gu et al., 1999; G. G. Cirino et al., 2014). The intervals every 25° ensured the smallest possible SZA variations and the largest possible number of points within the sample space necessary for statistical analyses. For each SZA interval analyzed, the average $\%NEE$ was evaluated in *bins* of f equal to 0.1, calculated separately (Figure 8). The critical points and the coefficients of curves for all data (between 0-75° SZA) are shown in the supplementary material (Figure S5, Table S2). On

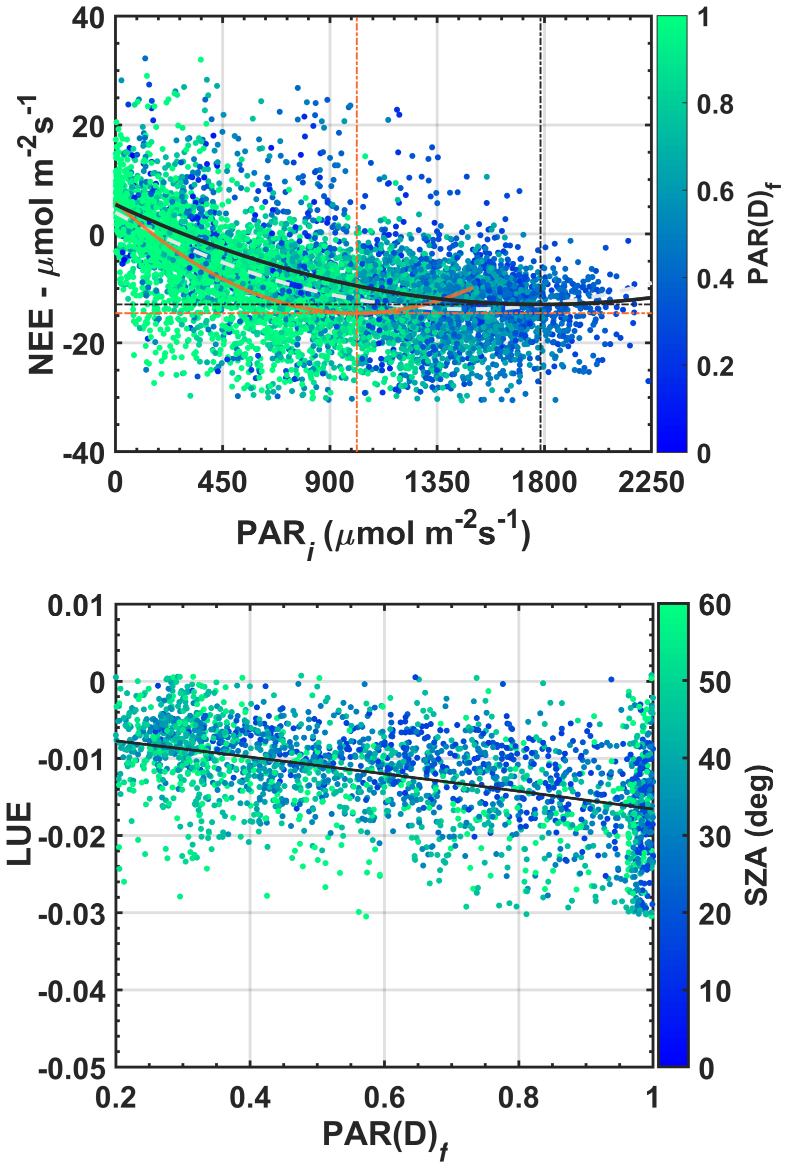

Figure 7. NEE as a function of radiation PAR$_i$ for measurements between 08h and 17h LT (top panel). The bottom panel shows the LUE as a function of the fraction $PAR(D)_f$ (R^2 = 0.21, the value of $p < 0.001$) for an area of semideciduous forest located in the municipality of Cláudia- MT, 50 km north of Sinop, between Jun2005-Jul2008.

average, an average (absolute) increase of approximately 7.0 μmol m^{-2}s^{-1} in carbon uptake was observed relative to clear sky conditions ($NEE(sza)_0$), when f varied from 1.1-1.0 to 0.66, results for the SZA range between 0-75° (Figure 8, top panel). The 7.0 μmol m^{-2}s^{-1} increase represents a 20-70% increase in NEE flux. This increase, strongly linked to the increase in aerosol concentration by fires, is mainly explained by the 50% increase in radiation $PAR(D)_f$ (approximately 450 μmol m^{-2}s^{-1} in the stream PAR_d) and 35-40% reduction in the irradiance f when the AOD$_a$ varies from 0.10 to 5.0 (Figure 5, bottom panel).

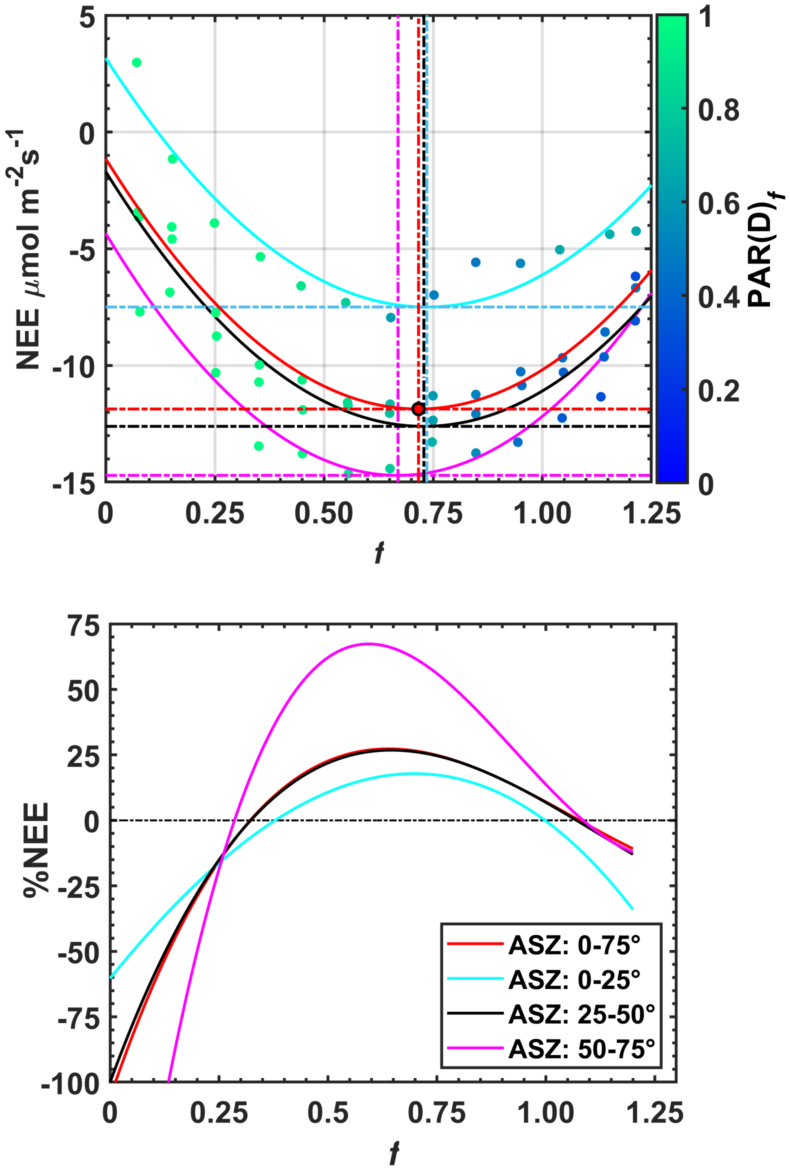

Figure 8. Variability of NEE with f for various SZA ranges in the top panel. The $\%NEE$ as a function of the irradiance f for the same SZA intervals is shown in the bottom panel. These graphs include the effects of aerosols in the experimental area of Cláudia-MT, between 2005-2008.

Oliveira et al. (2007) and (G. G. Cirino et al., 2014)(2014) showed a relative increase of about 30% for f values ranging from 1.1 to 0.80. The negative variations in f, also indicated a high pollution load for fires at the site (AOD between 0.10-2.5) (Figure 5, bottom panel) producing statistically significant reductions of up to 35% in the PAR radiation flux and a 47% increase in $PAR(D)_f$ (Figure 5, Figure 6, both bottom panel). These studies showed that the increase in carbon uptake, in the presence of aerosols and clouds, becomes smaller and similar in both locations for SZA bands < 20. Solar radiation suffers less scattering near the zenith ($SZA \sim 10°$) due to particles suspended in the atmosphere due to the narrowing of the optical path, reducing the effects of diffuse radiation on the photosynthetic process. These results, in particular, are generally repeated for the studied semi-deciduous forest of Mato Grosso, but a strong increase of 70% in $\%NEE$ is observed for lower SZA ranges (between 50-75%), in the early hours of the day, between 8-10h (LT), while in the Jaru Biological Reserve (JBR) the biggest increases are concentrated in the SZA ranges between 10-35°, close to midday, or in the morning-afternoon (Oliveira et al., 2007). At K34, in Manaus, the maximum absorptions and the maximum $\%NEE$ occur do not exceed 20% and the effects of aerosols and clouds operate together. The individual radiative influences of clouds and aerosols are difficult to quantify because satellite AOD observations have a low temporal resolution. Similar results were observed by Doughty et al. (2010) in FLONA-Tapajós, central Amazon. In general, higher standard deviations are found in regions most heavily impacted by aerosols, such as Ji-Paraná (RO) and Altafloresta (MT). Because aerosol concentrations are relatively lower in FLONA-Tapajós (PA) and Manaus (AM), the standard deviations are lower. Table 5 lists the coefficients of the adjustments found between $\%NEE$ and f for each of the considered ranges SZA, as well as the critical points (herein called biological optimum) for the irradiance values f and NEE flux (μmol m^{-2}s^{-1}).

These results are considered relevant, as a large part of the Amazon area is frequently impacted by the presence of aerosols in small amounts (low AOD), similar to those observed in the north of the Amazon basin, in Manaus-AM. In other regions, however, increases in the absorption of CO_2 are significant and can have major impacts on the carbon budget of the Amazon forest (as in the acro region of deforestation). Over dense forest ecosystems of central Amazonia, CO_2 absorption peaks are often observed at larger and narrower intervals, generally between 1.1 to 0.80; particularly observed value for dense forest ecosystems (Gu et al., 1999; Yamasoe et al., 2006; Oliveira et al., 2007; Doughty et al., 2010), and quite different from what is observed in grasslands and temperate forest regions of the world, where the maximum NEE (negative) is generally found in the range f between 1.0-0.5 (5-10 μmol m^{-2}s^{-1}) (Gu et al., 1999; Niyogi et al., 2004; Jing et al., 2010; Zhang et al., 2010).

The mechanisms used to explain the computation of the $\%NEE$ with the irradiance f is complex and also influenced by the dynamics of the Planetary Boundary Layer (PBL) throughout the day, including transport of regionally transported and locally emitted burning emissions. For the semideciduous forests studied here, an accumulation of aerosols from fires during the night hours (19h to 06h, LT) may be associated with greater stability in the PBL during the fire season (lower values in wind speed, reduction in convection and boundary layer narrowing). These factors can increase the concentration of aerosols (AOD_a) during the night hours, with important effects on the CO_2 absorption capacity ($\%NEE$) observed in the early hours of the day (SZA values between 50-75°. Given the dynamics of particulate transport (aerosol advection) from other regions to the experimental study area, higher CO2 absorption capacities ($\%NEE$) can be found in other types of forest ecosystems in the Amazon basin. Future studies may elucidate the dynamic effects of PBL on the photosynthetic capacity of forests in the Amazon Basin, like studies carried out in other forests around the world; in Wisconsin, EUA (Helliker & Ehleringer, 2000; Yakir, 2003); in Beijing, China (X. Wang et al., 2021; Z. Wang et al., 2022). Field experiments focused on radiative transfer from the leaf canopy, that is, on the vertical distribution of PAR_f radiation from the top to the top of the canopy, inside the forests, will improve the current understanding of the individual effects of aerosols and clouds on $\%NEE$ due to the cooling caused in Td_f and VPD, considered important biophysical variables essential for forest photosynthesis (ecosystem functioning).

3.6 Effects of fires on biophysical variables

Important direct interference of aerosols on environmental variables that consequently affect the photosynthetic dynamics of plants is observed in Figure 9 (von Randow et al., 2004; G. G. Cirino et al., 2014). The attenuating effect of incident solar irradiance due to the presence of aerosols triggers statistically significant reductions in air temperature

Table 5. Polynomial adjustments (Figure 8), coefficients, and statistics for the periods between 07-17h (LT) in the micrometeorological tower 50 km from Sinop-MT, in the municipality of Cláudia, between 2005-2008.

Settings	**Angles**	**Coefficients**				**Statistic**	
Poly fit 2nd	**ASZ**	***a***	***b***	***c***	***d***	$\mathbf{R^2}$	**C*p*** (x_v, y_v)
NEE	0-25°	+23	−31	−4.3		0.88	(0.74, -07.50)
	25-50°	+21	−30	−1.7		0.95	(0.73, -12.61)
	50-75°	+20	−29	+3.1		0.88	(0.67, -14.71)
	0-75°	+21	−30	−1.1		0.97	(0.72, -11.90)
Poly fit 3rd	**ASZ**	***a***	***b***	***c***	***d***	$\mathbf{R^2}$	**C*p*** (x_v, y_v)
%NEE	0-25°	−38	-1.1×10^2	$+2.1 \times 10^2$	−60	0.88	(0.70, 20.06)
	25-50°	$+1.5 \times 10^2$	-4.9×10^2	$+4.5 \times 10^2$	-1.0×10^2	0.97	(0.68, 26.68)
	50-75°	$+5.4 \times 10^2$	-1.5×10^3	$+1.2 \times 10^3$	-2.4×10^2	0.97	(0.58, 56.77)
	0-75°	$+1.7 \times 10^2$	-5.4×10^2	$+4.9 \times 10^2$	-1.1×10^2	0.98	(0.66, 27.05)

near the forest canopy. Several mechanisms have been used to explain the increase in photosynthetic capacity by the canopy due to changes in the biophysical properties of the forest, among them, the general trend of decreasing VPD (Vapour-Pressure Deficit) under cloudy or smoky skies (Min, 2005; Yuan et al., 2019) and cooldowns of up to 3–4 °C (Koren et al., 2014; Bai et al., 2012). In this present research, reductions in temperature and VPD, intrinsically linked to relative humidity, are also observed (Figure 9). In the semi-deciduous forest of Mato Grosso, the impact of aerosols produced, respectively, a cooling of 3 °C and 2.5 °C in Td_f and T_{ar} when f jumped from 1.1-1.10 to 0.66 (Figure 9, on top panel and middle panel). These results are similar to the results found by (Davidi et al., 2009). The effects of these coolings, especially in Td_f, could not be heated in isolation, but they can exert a large influence on the photosynthesis of the forest (Doughty et al., 2010), inducing positive variations in the flux $\%NEE$, considering the same variations pointed at f (Doughty et al., 2010).

Figure 9 (bottom panel) shows the relationship between the VPD and the irradiance f (this time, between SZA angles of 0-60°). For Freedman et al. (1998), the increase in relative humidity due to cooling induced by clouds and/or aerosols (Altaratz et al., 2008) can increase photosynthesis, as this increase naturally induces the opening of stomata of leaves (Collatz et al., 1991; Jing et al., 2010). In many forest locations, the reduction in f produces a decrease in VPD of around 35% during the dry season. These reductions, strongly influenced by the cooling of the air, are also closely linked with the cooling of the forest canopy and the increase in the absorption capacity of CO_2 ($\%NEE$) (Doughty et al., 2010). For cloudy and/or polluted sky conditions, generally decreasing VPD behavior can influence stomata opening and intensify photosynthesis (Jing et al., 2010). Studies focused on the impacts of fires on the flux of water to the atmosphere deserve attention and expansion in this sense. the results can help to understand the role of forests in maintaining rainfall and its effects on the hydrological cycle (studies not yet carried out for most biomes in the Amazon).

The results presented in Figure 9, viewed as a function of the frequency distribution of the clarity index kt, indicate that the current patterns of aerosol loading on the studied semideciduous forest ecosystem exceed the maximum limit for the which dense upland forests of central Amazônia reach the maximum amounts of carbon uptake (results not shown) (Oliveira et al., 2007; G. G. Cirino et al., 2014; Doughty et al., 2010). This scientific finding, in particular, apparently reveals greater tolerance (resilience) of semideciduous forests to aerosol loads by fires, considering the persistent and high loads of aerosols by fires in the Mato Grosso region over the last 30 years.

Unlike what was found here, the forests of central Amazonia, in Manaus-AM (K34), FLONA-Tapajós (K83), Santarém-PA and Ji-Paraná (RO) seem to be less tolerant to the attenuations of sunlight (induced by clouds and aerosols), required for the photosynthesis process. In the studied semideciduous forest, the distribution of kt is close to 0.66 for $\text{AOD}_a \gg 0.10$ Table 5. This value is 15-20% lower than the f values found in central Amazônia, when the NEE reaches maximum negative values during the burning season ($kt \sim 0.80$). This is the threshold value at which maximum carbon absorption is observed due to cloudiness and/or aerosol load in the JBR in the Ji-Paraná JBR (south of the Amazon basin) as well as in the Cuieiras reserve at K34, in Manaus-AM. These analyzes and comparisons are relevant because higher (lower) amounts of aerosols and clouds in the Amazon region can cause certain types of forests to absorb even higher (lower) amounts of carbon throughout the day, depending on fluctuations in light levels due to aerosols and clouds along the leaf canopy or in the regions between the ground and top of forests (Gu et al., 1999; G. G. Cirino et al., 2014). The kt frequency distribution patterns and their impacts on photosynthesis remain unknown for many other forest types in the Amazon and around the world. The results reported here for semideciduous forests in northern Mato Grosso are also consistent with calculations by Gu et al. (1999), for temperate forests in Canada, where negative maximums in NEE flux occur for ranges kt between 0.55– 0.60.

The interannual variability of the relationship between the observed AODa, fire counts and NEE could not be analyzed, mainly due to the lack of a long time series of NEE flux data in the region. In the central Amazon, significant variability was observed from year to year. Higher $\%NEE$ were often found on days with high fire counts. However, water stress and nutrient availability also play an important role in the carbon uptake capacity (Gatti et al., 2014; Hofhansl et al., 2016; Gatti et al., 2021; Malhi et al., 2021). Joint modifications in these variables make it extremely difficult to quantify the individual effects of aerosols and clouds on the NEE. Field experiments taking measurements of all these aspects will yield studies with more robust and comprehensive conclusions on the ecosystem responses of Amazonian forests to external environmental disturbances such as fires.

4 Conclusion

4.1 Challenges met

The aerosol optical depth derived from the AERONET system proved to be a satisfactory key variable in the elaboration of the clear sky solar irradiance model used to determine the relative irradiance f. The conceived model can be directed to other regions of the Amazon as long as they are within the same latitude range, where there are no SW_i measurements. In this study, it was possible to separate the radiative effects of aerosols from the effects produced by clouds, combining the measurements of incident solar radiation from the AERONET system with the AOD_a measurements.

The parameter f, allowed us to satisfactorily evaluate the radiative effects of aerosols from fires on the net absorption of carbon by the studied semideciduous forest ecosystem, absorption here represented by the NEE flux. The radiative impacts on the radiation fluxes PAR_i and PAR_d, allowed us to evaluate the impairment of the efficiency of light use by the forest (LUE), which increased by $\sim$ 1-3% under polluted conditions (AOD_a). The changes in incident solar radiation and CO_2 flux (NEE) could be attributed to the

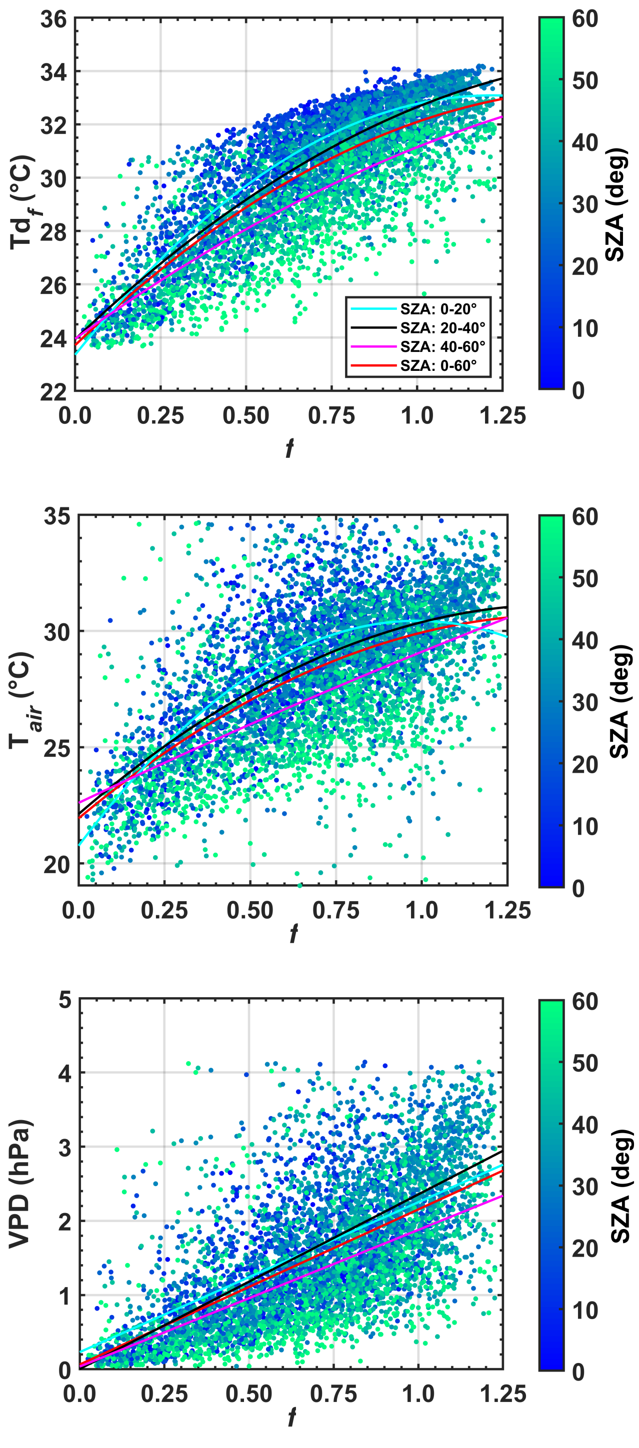

Figure 9. Correlation between the relative irradiance f with Td_f (top panel), T_{air} (middle panel) and VPD (bottom panel), values calculated for SZA between 0 and 60. The air temperature was measured at 42 m above the ground, in the micrometeorological tower located in the municipality of Cláudia, 50 km from Sinop-MT, using the parameterization given in Tribuzy (2005), between 2003-2004.

combined effects of aerosols emitted locally, regionally, or transported from more distant regions, considering the applied methods.

In the studied semideciduous forest ecosystem, the net carbon flux (NEE) increased from 20-70% when the optical depth varied from 0.1 to 5.0 (on average). This effect was attributed to an average reduction of up to 40% in the amount of total PAR radiation and also to an increase of up to 50% in the diffuse fraction of radiation ($PAR(D)_f$). This increase in CO_2 absorption capacity by the ecosystem is closely linked to the floristic composition of the understory and certain types of forest species adapted to low light conditions, which consists of more efficient vegetation in capturing diffused light. during the photosynthesis process. The results show higher photosynthetic efficiency under smoky sky conditions; loaded with particles scattering solar radiation due to fires, but also reveal the maximum limit in the PAR radiation cuts required for the photosynthesis process. Relative irradiances f less than 0.66, on average, indicate the critical point at which forest photosynthetic rates undergo drastic reductions. Irradiance values $f \sim$ of 0.22 indicate 100% interruption in the photosynthetic process.

Due to the increase in the concentration of aerosol particles from fires in the region, statistically, significant changes were also observed in meteorological (biophysical) variables such as leaf canopy temperature and VPD. Scientific findings reveal a strong influence of fire aerosols on these variables, with potentially important effects on photosynthesis and carbon absorption. The 3 and 5 °C reductions in leaf canopy and air temperature are strongly associated with a 40% reduction in f and a $\sim$ 2.0 mb reduction in VPD values which induce opening stomata and contribute to the observed increase of 20-70% in the CO_2 absorption capacity of the forest ($\%NEE$). The individual influences or contributions of the VPD, T_{air} and Td_f to the ecosystem's net balance of CO_2, however, could not be directly quantified in this research. Indirect correlations, however, reveal statistically significant effects between the mentioned biophysical variables and the observed changes in the NEE flux during the exposure of forests to fire and high values of AOD_a (greater than 1.25, on average).

4.2 Suggestions for future work

A more comprehensive regional study of the effects mentioned here, based on other vegetation types and biomes, using vegetation maps, remote sensing estimates, meteorological data, and numerical modeling, will help to better understand how the climate and ecosystem function in the Amazon are affected. affected by natural and anthropic environmental factors. The reductions in the NEE flux and, therefore, the reduction of the photosynthetic capacity of the plants due to the excessive increase in the concentration of BBOA aerosols and drastic reductions in the fluxes of solar radiation ($f \leq 0.22$) due to the fires in the region, constitutes an effect of notable relevance for carbon cycling in semi-deciduous forest environments in the Amazon and, therefore, an important contribution to a better understanding of this cycle in the region and the world.

Open Research Section

This section provides free access to data repositories that support the conclusions. Turbulent covariance data and Automatic Weather Systems, as well as selected formulas, will be available shortly on the Ameriflux website (https://ameriflux.lbl.gov) according to Vourlitis et al. (2011): "Temporal patterns of net CO_2 exchange for a semideciduous tropical forest in the southern Amazon Basin". Alternatively, we provide the data from this survey available through the Mendeley Data platform (https://data.mendeley.com), where we will make upgrades and possible corrections. Citation: Cirino, Glauber; Vourlitis, George; Silva, Simone; Palácios, Rafael (2022), "Brazil-FluxMet-Stf", Mendeley Data, v1 DOI: 10.17632/m5h5fw872g.1. Secondary data is already in the public domain. We have listed the links to these data in the Supporting Information (Table S3).

Acknowledgments

We want to thank The National Science Foundation, National Council for Scientific and Technological Development (CNPq), and Foundation for Research Support of the State of Mato Grosso (FAPEMAT), California State University, San Marcos (CSUSM), the Federal University of Mato Grosso (UFMT) and the Union of Lumberjacks of Northern Mato Grosso (SINDUSMAD) by the funding support provided. Additional funding was provided by the CNPq Universal, project 422894/2021-4, and the Pará State Research Support Foundation (FAPESPA), grant 2022/45107. Our special thanks to Professor Dr. José de Souza Nogueira *(in memoriam)* who worked with other collaborators to generate and obtain the micrometeorological data from the measurement tower used in this research.

References

Ackerly, D. D., Thomas, W. M. W., Ferreira, C. A. C. I. D., & Pirani, J. R. (1989). The forest-cerrado transition zone in southern Amazonia: results of the 1985 project flora amazonica expedition to Mato Grosso. , *41*(2), 113–128.

Adachi, K., Oshima, N., Gong, Z., de Sá, S., Bateman, A. P., Martin, S. T., ... Buseck, P. R. (2020). Mixing states of Amazon basin aerosol particles transported over long distances using transmission electron microscopy. *Atmospheric Chemistry and Physics*, *20*(20), 11923–11939. Retrieved from https://acp.copernicus.org/articles/20/11923/2020/ doi: 10.5194/acp-20-11923-2020

Alencar, A. A. C., Arruda, V. L. S., Silva, W. V. d., Conciani, D. E., Costa, D. P., Crusco, N., ... Vélez-Martin, E. (2022). Long-term landsat-based monthly burned area dataset for the brazilian biomes using deep learning. *Remote Sensing*, *14*(11). Retrieved from https://www.mdpi.com/2072-4292/14/11/2510 doi: 10.3390/rs14112510

Altaratz, O., Koren, I., & Reisin, T. (2008). Humidity impact on the aerosol effect in warm cumulus clouds. *Geophysical Research Letters*, *35*(17), 1–5. doi: 10.1029/2008GL034178

Amorim Neto, A. d. C., Satyamurty, P., & Correia, F. W. (2015). Some observed characteristics of frontal systems in the amazon basin. *Meteorological Applications*, *22*(3), 617-635. Retrieved from https://rmets.onlinelibrary.wiley.com/doi/abs/10.1002/met.1497 doi: https://doi.org/10.1002/met.1497

Aragão, L. E., Anderson, L. O., Fonseca, M. G., Rosan, T. M., Vedovato, L. B., Wagner, F. H., ... Saatchi, S. (2018). 21st Century drought-related fires counteract the decline of Amazon deforestation carbon emissions. *Nature Communications*, *9*(1), 1–12. Retrieved from http://dx.doi.org/10.1038/s41467-017-02771-y doi: 10.1038/s41467-017-02771-y

Araújo, A. C., Dolman, A. J., Waterloo, M. J., Gash, J. H., Kruijt, B., Zanchi, F. B., ... Backer, J. (2010). The spatial variability of CO2 storage and the interpretation of eddy covariance fluxes in central Amazonia. *Agricultural and Forest Meteorology*, *150*(2), 226–237. doi: 10.1016/j.agrformet.2009.11.005

Artaxo, P., Mohr, C., & Pöschl, U. (2022). Tropical and Boreal Forest – Atmosphere Interactions : A Review. , *74*, 24–163. doi: 10.16993/tellusb.34

Artaxo, P., Rizzo, L. V., Brito, J. F., Barbosa, H. M., Arana, A., Sena, E. T., ... Andreae, M. O. (2013). Atmospheric aerosols in Amazonia and land use change: From natural biogenic to biomass burning conditions. *Faraday Discussions*, *165*(February 2014), 203–235. doi: 10.1039/c3fd00052d

Aubinet, M. (2012). *Eddy Covariance.* doi: 10.1007/978-94-007-2351-1

Aubinet, M., Chermanne, B., Vandenhaute, M., Longdoz, B., Yernaux, M., & Laitat, E. (2001). Long term carbon dioxide exchange above a mixed forest in the Belgian Ardennes. *Agricultural and Forest Meteorology*, *108*(4), 293–315. doi: 10.1016/S0168-1923(01)00244-1

Avitabile, V., Herold, M., Heuvelink, G. B., Lewis, S. L., Phillips, O. L., Asner, G. P., ... Willcock, S. (2016). An integrated pan-tropical biomass map using multiple reference datasets. *Global Change Biology*, *22*(4), 1406–1420. doi: 10.1111/gcb.13139

Bai, Y., Wang, J., Zhang, B., Zhang, Z., & Liang, J. (2012). Comparing the impact of cloudiness on carbon dioxide exchange in a grassland and a maize cropland in northwestern China. *Ecological Research*, *27*(3), 615–623. doi: 10.1007/s11284-012-0930-z

Balch, J. K., Brando, P. M., Nepstad, D. C., Coe, M. T., Silvério, D., Massad, T. J., ... Carvalho, K. S. (2015). The Susceptibility of Southeastern Amazon Forests to Fire: Insights from a Large-Scale Burn Experiment. *BioScience*, *65*(9), 893–905. doi: 10.1093/biosci/biv106

Beer, C., Reichstein, M., Tomelleri, E., Ciais, P., Jung, M., Carvalhais, N., ... Papale, D. (2010). Terrestrial gross carbon dioxide uptake: Global distribution and covariation with climate. *Science*, *329*(5993), 834–838. doi: 10.1126/science.1184984

Bian, H., Lee, E., Koster, R. D., Barahona, D., Chin, M., Colarco, P. R., ... Zeng, F. (2021). The response of the Amazon ecosystem to the photosynthetically active radiation fields: Integrating impacts of biomass burning aerosol and clouds in the NASA GEOS Earth system model. *Atmospheric Chemistry and Physics*, *21*(18), 14177–14197. doi: 10.5194/acp-21-14177-2021

Booth, B. B., Jones, C. D., Collins, M., Totterdell, I. J., Cox, P. M., Sitch, S., ... Lloyd, J. (2012). High sensitivity of future global warming to land carbon cycle processes. *Environmental Research Letters*, *7*(2). doi: 10.1088/1748-9326/7/2/024002

Braghiere, Kerches Renato, Akemi Yamasoe, M., Manuel Évora do RosáRio, N., Ribeiro Da Rocha, H., De Souza Nogueira, J., & Carioca de AraÚJo, A. (2020). Characterization of the radiative impact of aerosols on CO2 and energy fluxes in the Amazon deforestation arch using artificial neural networks. *Atmospheric Chemistry and Physics*, *20*(6), 3439–3458. doi: 10.5194/acp-20-3439-2020

Brienen, R. J., Phillips, O. L., Feldpausch, T. R., Gloor, E., Baker, T. R., Lloyd, J., ... Zagt, R. J. (2015). Long-term decline of the Amazon carbon sink. *Nature*, *519*(7543), 344–348. Retrieved from http://dx.doi.org/10.1038/nature14283 doi: 10.1038/nature14283

Burba, G. (2013). *Eddy covariance method for scientific, industrial, agricultural and regulatory applications: A field book on measuring ecosystem gas exchange and areal emission rates.* doi: 10.13140/RG.2.1.4247.8561

Carswell, F. E., Costa, A. L., Palheta, M., Malhi, Y., Meir, P., Costa, J. d. P. R., ... Grace, J. (2002). Seasonality in co2 and h2o flux at an eastern amazonian rain forest. *Journal of Geophysical Research: Atmospheres*, *107*(D20), LBA 43-1-LBA 43-16. Retrieved from https://agupubs.onlinelibrary.wiley.com/doi/abs/10.1029/2000JD000284 doi: https://doi.org/10.1029/2000JD000284

Cirino, G., Brito, J., Barbosa, H. M., Rizzo, L. V., Tunved, P., de Sá, S. S., ... Artaxo, P. (2018). Observations of Manaus urban plume evolution and interaction with biogenic emissions in GoAmazon 2014/5. *Atmospheric Environment*, *191*(August), 513–524. doi: 10.1016/j.atmosenv.2018.08.031

Cirino, G. G., Souza, R. A., Adams, D. K., & Artaxo, P. (2014). The effect of atmospheric aerosol particles and clouds on net ecosystem exchange in the Amazon. *Atmospheric Chemistry and Physics*, *14*(13), 6523–6543. doi: 10.5194/acp-14-6523-2014

Collatz, G. J., Ball, J. T., Grivet, C., & Berry, J. A. (1991). Physiological and environmental regulation of stomatal conductance, photosynthesis and transpiration: a model that includes a laminar boundary layer. *Agricultural and*

Forest Meteorology, *54*(2-4), 107–136. doi: 10.1016/0168-1923(91)90002-8

Davidi, A., Koren, I., & Remer, L. (2009). Direct measurements of the effect of biomass burning over the Amazon on the atmospheric temperature profile. *Atmospheric Chemistry and Physics*, *9*(21), 8211–8221. doi: 10.5194/acp-9-8211-2009

de Magalhães, N., Evangelista, H., Condom, T., Rabatel, A., & Ginot, P. (2019). Amazonian Biomass Burning Enhances Tropical Andean Glaciers Melting. *Scientific Reports*, *9*(1), 1–12. doi: 10.1038/s41598-019-53284-1

de Sá, S. S., Rizzo, L. V., Palm, B. B., Campuzano-Jost, P., Day, D. A., Yee, L. D., … Martin, S. T. (2019). Contributions of biomass-burning, urban, and biogenic emissions to the concentrations and light-absorbing properties of particulate matter in central amazonia during the dry season. *Atmospheric Chemistry and Physics*, *19*(12), 7973–8001. Retrieved from https://acp.copernicus.org/articles/19/7973/2019/ doi: 10.5194/acp-19-7973-2019

Doughty, C. E., Flanner, M. G., & Goulden, M. L. (2010). Effect of smoke on subcanopy shaded light, canopy temperature, and carbon dioxide uptake in an Amazon rainforest. *Global Biogeochemical Cycles*, *24*(3), 1–10. doi: 10.1029/2009GB003670

Doughty, C. E., Metcalfe, D. B., Girardin, C. A., Amézquita, F. F., Cabrera, D. G., Huasco, W. H., … Malhi, Y. (2015). Drought impact on forest carbon dynamics and fluxes in Amazonia. *Nature*, *519*(7541), 78–82. doi: 10.1038/nature14213

Finnigan, J. (2006). The storage term in eddy flux calculations. *Agricultural and Forest Meteorology*, *136*(3-4), 108–113. doi: 10.1016/j.agrformet.2004.12.010

Foken, T. (2008). *Micrometeorology.* Springer Berlin Heidelberg. doi: 10.1007/978-3-540-74666-9

Freedman, J., Fitzjarrald, D., Moore, K., & Sakai, R. (1998). Boundary layer cloud climatology and enhanced forest-atmosphere exchange. In *Preprints of 23rd conference on agricultural and forest meteorology* (pp. 41–44).

Fu, Z., Gerken, T., Bromley, G., Araújo, A., Bonal, D., Burban, B., … Stoy, P. C. (2018). The surface-atmosphere exchange of carbon dioxide in tropical rainforests: Sensitivity to environmental drivers and flux measurement methodology. *Agricultural and Forest Meteorology*, *263*(December 2017), 292–307. Retrieved from https://doi.org/10.1016/j.agrformet.2018.09.001 doi: 10.1016/j.agrformet.2018.09.001

Gao, Y. (2020). Atmospheric Aerosols Elevated Ecosystem Productivity of a Poplar Plantation in Beijing, 2 China.

Gates, D. M. (1980). *Biophysical Ecology.*

Gatti, L. V., Basso, L. S., Miller, J. B., Gloor, M., Gatti Domingues, L., Cassol, H. L., … Neves, R. A. (2021). Amazonia as a carbon source linked to deforestation and climate change. *Nature*, *595*(7867), 388–393. Retrieved from http://dx.doi.org/10.1038/s41586-021-03629-6 doi: 10.1038/s41586-021-03629-6

Gatti, L. V., Gloor, M., Miller, J. B., Doughty, C. E., Malhi, Y., Domingues, L. G., … Lloyd, J. (2014). Drought sensitivity of Amazonian carbon balance revealed by atmospheric measurements. *Nature*, *506*(7486), 76–80. Retrieved from http://dx.doi.org/10.1038/nature12957 doi: 10.1038/nature12957

Goulden, M. L., Miller, S. D., Da Rocha, H. R., Menton, M. C., De Freitas, H. C., E Silva Figueira, A. M., & Dias De Sousa, C. A. (2004). Diel and seasonal patterns of tropical forest CO2 exchange. *Ecological Applications*, *14*(4 SUPPL.), 42–54. doi: 10.1890/02-6008

Grace, J., Malhi, Y., Lloyd, J., McIntyre, J., Miranda, A. C., Meir, P., & Miranda, H. S. (1996). The use of eddy covariance to infer the net carbon dioxide uptake of Brazilian rain forest. *Global Change Biology*, *2*(3), 209–217. doi:

10.1111/j.1365-2486.1996.tb00073.x

Gu, L., Fuentes, J. D., Garstang, M., Silva, J. T. D., Heitz, R., Sigler, J., & Shugart, H. H. (2001). Cloud modulation of surface solar irradiance at a pasture site in Southern Brazil. *Agricultural and Forest Meteorology*, *106*(2), 117–129. doi: 10.1016/S0168-1923(00)00209-4

Gu, L., Fuentes, J. D., Shugart, H. H., Staebler, R. M., & Black, T. A. (1999). Responses of net ecosystem exchanges of carbon dioxide to changes in cloudiness: Results from two North American deciduous forests. *Journal of Geophysical Research Atmospheres*, *104*(D24), 31421–31434. doi: 10.1029/1999JD901068

Helliker, B. R., & Ehleringer, J. R. (2000). Establishing a grassland signature in veins: ¡sup¿18¡/sup¿o in the leaf water of c¡sub¿3¡/sub¿ and c¡sub¿4¡/sub¿ grasses. *Proceedings of the National Academy of Sciences*, *97*(14), 7894-7898. Retrieved from https://www.pnas.org/doi/abs/10.1073/pnas.97.14.7894 doi: 10.1073/pnas.97.14.7894

Hofhansl, F., Andersen, K. M., Fleischer, K., Fuchslueger, L., Rammig, A., Schaap, K. J., ... Lapola, D. M. (2016). Amazon forest ecosystem responses to elevated atmospheric Co2 and alterations in nutrient availability: Filling the gaps with model-experiment integration. *Frontiers in Earth Science*, *4*(February), 1–9. doi: 10.3389/feart.2016.00019

Holben, B. N., Eck, T. F., Slutsker, I., Tanré, D., Buis, J. P., Setzer, A., ... Smirnov, A. (1998). AERONET - A federated instrument network and data archive for aerosol characterization. *Remote Sensing of Environment*, *66*(1), 1–16. doi: 10.1016/S0034-4257(98)00031-5

Hollinger, D. Y., & Richardson, A. D. (2005). Uncertainty in eddy covariance measurements and its application to physiological models. , 873–885.

Huntingford, C., Zelazowski, P., Galbraith, D., Mercado, L. M., Sitch, S., Fisher, R., ... Cox, P. M. (2013). Simulated resilience of tropical rainforests to CO2 -induced climate change. *Nature Geoscience*, *6*(4), 268–273. Retrieved from http://dx.doi.org/10.1038/ngeo1741 doi: 10.1038/ngeo1741

Jing, X., Huang, J., Wang, G., Higuchi, K., Bi, J., Sun, Y., ... Wang, T. (2010). The effects of clouds and aerosols on net ecosystem CO 2 exchange over semi-arid Loess Plateau of Northwest China. *Atmospheric Chemistry and Physics*, *10*(17), 8205–8218. doi: 10.5194/acp-10-8205-2010

Kanniah, K. D., Beringer, J., North, P., & Hutley, L. (2012). Control of atmospheric particles on diffuse radiation and terrestrial plant productivity: A review. *Progress in Physical Geography*, *36*(2), 209–237. doi: 10.1177/0309133311434244

Koren, I., Dagan, G., & Altaratz, O. (2014). From aerosol-limited to invigoration of warm convective clouds. *Science*, *344*(6188), 1143–1146. doi: 10.1126/science.1252595

Levy, R. C., Mattoo, S., Munchak, L. A., Remer, L. A., Sayer, A. M., Patadia, F., & Hsu, N. C. (2013). The Collection 6 MODIS aerosol products over land and ocean. *Atmospheric Measurement Techniques*, *6*(11), 2989–3034. doi: 10.5194/amt-6-2989-2013

Lorenzi, H. (2000). *Arvores , brasileiras.* São Paulo.

Lorenzi, H. (2002). *Arvores , brasileiras* (L. Instituto Plantarum de Estudos da Flora, Ed.). Sao Paulo.

Malavelle, F. F., Haywood, J. M., Mercado, L. M., Folberth, G. A., Bellouin, N., Sitch, S., & Artaxo, P. (2019). Studying the impact of biomass burning aerosol radiative and climate effects on the Amazon rainforest productivity with an Earth system model. *Atmospheric Chemistry and Physics*, *19*(2), 1301–1326. doi: 10.5194/acp-19-1301-2019

Malhi, Y., Melack, J., Gatti, L. V., Ometto, J. P., Kesselmeier, J., Wolff, S., ... Silva Junior, C. H. L. (2021). *Chapter 6: Biogeochemical Cycles in the Amazon.* doi: 10.55161/takr3454

Martin, S. T., Andreae, M. O., Althausen, D., Artaxo, P., Baars, H., Borrmann, S., ... Zorn, S. R. (2010). An overview of the Amazonian Aerosol Characterization Experiment 2008 (AMAZE-08). *Atmospheric Chemistry and Physics*, *10*(23), 11415–11438. doi: 10.5194/acp-10-11415-2010

Martin, S. T., Andreae, M. O., Artaxo, P., Baumgardner, D., Chen, Q., Goldstein, A. H., ... Trebs, I. (2010). Sources and properties of Amazonian aerosol particles. *Reviews of Geophysics*, *48*(2). doi: 10.1029/2008RG000280

MATLAB. (2013). *version 9.8.8.748 (r2013a).* Natick, Massachusetts: The MathWorks Inc.

Mercado, L. M., Bellouin, N., Sitch, S., Boucher, O., Huntingford, C., Wild, M., & Cox, P. M. (2009). Impact of changes in diffuse radiation on the global land carbon sink. *Nature*, *458*(7241), 1014–1017. doi: 10.1038/nature07949

Meyers, T. P., & Dale, R. F. (1983). *Predicting daily insolation with hourly cloud height and coverage.* (Vol. 22) (No. 4). doi: 10.1175/1520-0450(1983)022⟨0537:PDIWHC⟩2.0.CO;2

Min, Q. (2005). Impacts of aerosols and clouds on forest-atmosphere carbon exchange. *Journal of Geophysical Research: Atmospheres*, *110*(D6). Retrieved from https://agupubs.onlinelibrary.wiley.com/doi/abs/10.1029/2004JD004858 doi: https://doi.org/10.1029/2004JD004858

Moncrieff, J. B., Massheder, J. M., De Bruin, H., Elbers, J., Friborg, T., Heusinkveld, B., ... Verhoef, A. (1997). A system to measure surface fluxes of momentum, sensible heat, water vapour and carbon dioxide. *Journal of Hydrology*, *188-189*(1-4), 589–611. doi: 10.1016/S0022-1694(96)03194-0

Montagnani, L., Grünwald, T., Kowalski, A., Mammarella, I., Merbold, L., Metzger, S., ... Siebicke, L. (2018). Estimating the storage term in eddy covariance measurements: The ICOS methodology. *International Agrophysics*, *32*(4), 551–567. doi: 10.1515/intag-2017-0037

Moreira, D. S., Freitas, S. R., Bonatti, J. P., Mercado, L. M., É. Rosário, N. M., Longo, K. M., ... Gatti, L. V. (2013). Coupling between the JULES land-surface scheme and the CCATT-BRAMS atmospheric chemistry model (JULES-CCATT-BRAMS1.0): Applications to numerical weather forecasting and the CO2 budget in South America. *Geoscientific Model Development*, *6*(4), 1243–1259. doi: 10.5194/gmd-6-1243-2013

Moreira, D. S., Longo, K. M., Freitas, S. R., Yamasoe, M. A., Mercado, L. M., Rosário, N. E., ... Correia, C. C. (2017). Modeling the radiative effects of biomass burning aerosols on carbon fluxes in the Amazon region. *Atmospheric Chemistry and Physics*, *17*(23), 14785–14810. doi: 10.5194/acp-17-14785-2017

Morgan, W. T., Darbyshire, E., Spracklen, D. V., Artaxo, P., & Coe, H. (2019). Non-deforestation drivers of fires are increasingly important sources of aerosol and carbon dioxide emissions across Amazonia. *Scientific Reports*, *9*(1), 1–15. Retrieved from http://dx.doi.org/10.1038/s41598-019-53112-6 doi: 10.1038/s41598-019-53112-6

Murphy, P. G., & Lugo, A. E. (1986). Ecology of tropical dry forest. *Annual review of ecology and systematics. Vol. 17*(November 2003), 67–88. doi: 10.1146/annurev.es.17.110186.000435

Nagy, L., Artaxo, P., & Forsberg, B. R. (2016). *Interactions Between Biosphere, Atmosphere, and Human Land Use in the Amazon Basin: An Introduction.* doi: 10.1007/978-3-662-49902-3_1

Nagy, R. C., Porder, S., Brando, P., Davidson, E. A., Figueira, A. M. e. S., Neill, C., ... Trumbore, S. (2018). Soil carbon dynamics in soybean cropland and forests in mato grosso, brazil. *Journal of Geophysical Research: Biogeosciences*, *123*(1), 18-31. Retrieved from https://agupubs.onlinelibrary.wiley.com/doi/abs/10.1002/2017JG004269 doi: https://doi.org/10.1002/2017JG004269

Nepstad, D., McGrath, D., Stickler, C., Alencar, A., Azevedo, A., Swette, B., … Hess, L. (2014). Slowing Amazon deforestation through public policy and interventions in beef and soy supply chains. *Science*, *344*(6188), 1118–1123. doi: 10.1126/science.1248525

Niyogi, D., Chang, H. I., Saxena, V. K., Holt, T., Alapaty, K., Booker, F., … Xue, Y. (2004). Direct observations of the effects of aerosol loading on net ecosystem CO_2 exchanges over different landscapes. *Geophysical Research Letters*, *31*(20), 1–5. doi: 10.1029/2004GL020915

Nogueira, E. M., Nelson, B. W., Fearnside, P. M., França, M. B., & de Oliveira, Á. C. A. (2008). Tree height in Brazil's 'arc of deforestation': Shorter trees in south and southwest Amazonia imply lower biomass. *Forest Ecology and Management*, *255*(7), 2963–2972. doi: 10.1016/j.foreco.2008.02.002

Oliveira, P. H., Artaxo, P., Pires, C., De Lucca, S., Procópio, A., Holben, B., … Rocha, H. R. (2007). The effects of biomass burning aerosols and clouds on the CO_2 flux in Amazonia. *Tellus, Series B: Chemical and Physical Meteorology*, *59*(3), 338–349. doi: 10.1111/j.1600-0889.2007.00270.x

Oliveira-Filho AT, R. J., & Oliveira. (2002). *The Cerrados of Brazil* (Vol. 20) (No. 11). Nova York. doi: 10.1258/ijsa.2009.009019

Pan, Y. (2011). A large and persistent carbon sink in the world's forests. *Science*, *333*(August), 988–993.

Prado, D. E., & Gibbs, P. E. (1993). Patterns of Species Distributions in the Dry Seasonal Forests of South America. *Annals of the Missouri Botanical Garden*, *80*(4), 902. doi: 10.2307/2399937

Procopio, A. S., Artaxo, P., Kaufman, Y. J., Remer, L. A., Schafer, J. S., & Holben, B. N. (2004). Multiyear analysis of amazonian biomass burning smoke radiative forcing of climate. *Geophysical Research Letters*, *31*(3), 1–4. doi: 10.1029/2003GL018646

Rap, A. (2015). Fires increase Amazon forest productivity. *Geophysical Research Letters*(June), 4654–4662. doi: 10.1002/2015GL063719.Received

Rap, A., Scott, C. E., Reddington, C. L., Mercado, L., Ellis, R. J., Garraway, S., … Spracklen, D. V. (2018). Enhanced global primary production by biogenic aerosol via diffuse radiation fertilization. *Nature Geoscience*, *11*(9), 640–644. Retrieved from http://dx.doi.org/10.1038/s41561-018-0208-3 doi: 10.1038/s41561-018-0208-3

Ratter, J. A., Askew, G. P., Montgomery, R. F., & Gifford, D. R. (1978). Observations on the vegetation of northeastern Mato Grosso II. Forests and soils of the Rio Suiá–Missu area. *Proceedings of the Royal Society of London. Series B, Containing papers of a Biological character. Royal Society (Great Britain)*, *203*(1151), 191–208. doi: 10.1098/rspb.1978.0100

Reindl, D., Beckman, W., & Duffie, J. (1990). Diffuse fraction correlations. *Solar Energy*, *45*(1), 1-7. Retrieved from https://www.sciencedirect.com/science/article/pii/0038092X9090060P doi: https://doi.org/10.1016/0038-092X(90)90060-P

Remer, L. A., Kaufman, Y. J., Tanré, D., Mattoo, S., Chu, D. A., Martins, J. V., … Holben, B. N. (2005). The MODIS aerosol algorithm, products, and validation. *Journal of the Atmospheric Sciences*, *62*(4), 947–973. doi: 10.1175/JAS3385.1

Remer, L. A., Mattoo, S., Levy, R. C., & Munchak, L. A. (2013). MODIS 3 km aerosol product: Algorithm and global perspective. *Atmospheric Measurement Techniques*, *6*(7), 1829–1844. doi: 10.5194/amt-6-1829-2013

Saatchi, S. S., Harris, N. L., Brown, S., Lefsky, M., Mitchard, E. T., Salas, W., … Morel, A. (2011). Benchmark map of forest carbon stocks in tropical regions across three continents. *Proceedings of the National Academy of Sciences of the United States of America*, *108*(24), 9899–9904. doi: 10.1073/pnas.1019576108

Saraiva, I., Silva Dias, M. A., Morales, C. A., & Saraiva, J. M. (2016). Regional variability of rain clouds in the amazon basin as seen by a network of weather radars. *Journal of Applied Meteorology and Climatology*, *55*(12), 2657–2675. doi: 10.1175/JAMC-D-15-0183.1

Schafer, J. S., Eck, T. F., Holben, B. N., Artaxo, P., & Duarte, A. F. (2008). Characterization of the optical properties of atmospheric aerosols in Amazônia from long-term AERONET monitoring (1993-1995 and 1999-2006). *Journal of Geophysical Research Atmospheres*, *113*(4), 1–16. doi: 10.1029/2007JD009319

Schafer, J. S., Eck, T. F., Holben, B. N., Artaxo, P., Yamasoe, M. A., & Procopio, A. S. (2002). Observed reductions of total solar irradiance by biomass-burning aerosols in the Brazilian Amazon and Zambian Savanna. *Geophysical Research Letters*, *29*(17), 2–5. doi: 10.1029/2001GL014309

Schafer, J. S., Holben, B. N., Eck, T. F., Yamasoe, M. A., & Artaxo, P. (2002). Atmospheric effects on insolation in the Brazilian Amazon: Observed modification of solar radiation by clouds and smoke and derived single scattering albedo of fire aerosols. *Journal of Geophysical Research: Atmospheres*, *107*(20), LBA 41–1–LBA 41–15. doi: 10.1029/2001JD000428

Schuepp, P. H., Leclerc, M. Y., MacPherson, J. I., & Desjardins, R. L. (1990). Footprint prediction of scalar fluxes from analytical solutions of the diffusion equation. *Boundary-Layer Meteorology*, *50*(1-4), 355–373. doi: 10.1007/BF00120530

Shilling, J. E., Pekour, M. S., Fortner, E. C., Artaxo, P., de Sá, S., Hubbe, J. M., ... Wang, J. (2018). Aircraft observations of the chemical composition and aging of aerosol in the manaus urban plume during goamazon 2014/5. *Atmospheric Chemistry and Physics*, *18*(14), 10773–10797. Retrieved from https://acp.copernicus.org/articles/18/10773/2018/ doi: 10.5194/acp-18-10773-2018

Silva, C. V., Aragão, L. E., Young, P. J., Espirito-Santo, F., Berenguer, E., Anderson, L. O., ... Barlow, J. (2020). Estimating the multi-decadal carbon deficit of burned Amazonian forests. *Environmental Research Letters*, *15*(11). doi: 10.1088/1748-9326/abb62c

Spitters, C. J., Toussaint, H. A., & Goudriaan, J. (1986). Separating the diffuse and direct component of global radiation and its implications for modeling canopy photosynthesis Part I. Components of incoming radiation. *Agricultural and Forest Meteorology*, *38*(1-3), 217–229. doi: 10.1016/0168-1923(86)90060-2

Tribuzy, E. S. (2005). Canopy leaf temperature variations and their effect on the CO2 assimilation rate in Central Amazonia (in Portuguese). *Doctoral thesis*, 102.

von Randow, C., Manzi, A. O., Kruijt, B., de Oliveira, P. J., Zanchi, F. B., Silva, R. L., ... Kabat, P. (2004). Comparative measurements and seasonal variations in energy and carbon exchange over forest and pasture in South West Amazonia. *Theoretical and Applied Climatology*, *78*(1-3), 5–26. doi: 10.1007/s00704-004-0041-z

Vourlitis, G. L., De Almeida Lobo, F., Zeilhofer, P., & De Souza Nogueira, J. (2011). Temporal patterns of net CO2 exchange for a tropical semideciduous forest of the southern Amazon Basin. *Journal of Geophysical Research: Biogeosciences*, *116*(3), 1–15. doi: 10.1029/2010JG001524

Vourlitis, G. L., Priante Filho, N., Hayashi, M. M., Nogueira, J. D. S., Caseiro, F. T., & Campelo, J. H. (2002). Seasonal variations in the evapotranspiration of a transitional tropical forest of Mato Grosso, Brazil. *Water Resources Research*, *38*(6), 30–1–30–11. doi: 10.1029/2000wr000122

Vourlitis, G. L., Priante Filho, N., Hayashi, M. M., Nogueira, J. D. S., Caseiro, F. T., & Holanda Campelo, J. (2001). Seasonal variations in the net ecosystem CO2 exchange of a mature Amazonian transitional tropical forest (cerradão). *Functional Ecology*, *15*(3), 388–395. doi: 10.1046/j.1365-2435.2001.00535.x

Wang, X., Wang, C., Wu, J., Miao, G., Chen, M., Chen, S., ... Liu, L. (2021). Intermediate aerosol loading enhances photosynthetic activity of croplands. *Geophysical Research Letters*, *48*(7), e2020GL091893. Retrieved from https://agupubs.onlinelibrary.wiley.com/doi/abs/10.1029/2020GL091893 (e2020GL091893 2020GL091893) doi: https://doi.org/10.1029/2020GL091893

Wang, Z., Wang, C., Wang, X., Wang, B., Wu, J., & Liu, L. (2022). Aerosol pollution alters the diurnal dynamics of sun and shade leaf photosynthesis through different mechanisms. *Plant, Cell & Environment*, *45*(10), 2943-2953. Retrieved from https://onlinelibrary.wiley.com/doi/abs/10.1111/pce.14411 doi: https://doi.org/10.1111/pce.14411

Yakir, D. (2003). 4.07 - the stable isotopic composition of atmospheric co2. In H. D. Holland & K. K. Turekian (Eds.), *Treatise on geochemistry* (p. 175-212). Oxford: Pergamon. Retrieved from https://www.sciencedirect.com/science/article/pii/B008043751604038X doi: https://doi.org/10.1016/B0-08-043751-6/04038-X

Yamasoe, M. A., Randow, C. V., Manzi, A. O., Schafer, J. S., Eck, T. F., & Holben, B. N. (2006). Effect of smoke and clouds on the transmissivity of photosynthetically active radiation inside the canopy. , 1645–1656.

Yuan, W., Zheng, Y., Piao, S., Ciais, P., Lombardozzi, D., Wang, Y., ... Yang, S. (2019). Increased atmospheric vapor pressure deficit reduces global vegetation growth. *Science Advances*, *5*(8), 1–13. doi: 10.1126/sciadv.aax1396

Zhang, M., Yu, G. R., Zhang, L. M., Sun, X. M., Wen, X. F., Han, S. J., & Yan, J. H. (2010). Impact of cloudiness on net ecosystem exchange of carbon dioxide in different types of forest ecosystems in China. *Biogeosciences*, *7*(2), 711–722. doi: 10.5194/bg-7-711-2010

JOURNAL OF GEOPHYSICAL RESEARCH

Supporting Information for "Enhanced net CO_2 exchange of a semi-deciduous forest in the southern Amazon due to diffuse radiation from biomass burning"

S. N. R. Silva[1], G. G. Cirino[2,1,5], D. S. Moreira[3], R. S. Palácios[2,5], M. I. Vitorino[1,2], and G. L. Vourlitis[4]

[1]Programa de Pós-Graduação em Ciências Ambientais, Universidade Federal do Pará, Belém-PA, Brazil

[2]Instituto de Geociências, Faculdade de Meteorologia, Universidade Federal do Pará, Belém-PA, Brazil

[3]Faculdade de Ciências, Universidade Estadual Paulista, Bauru-SP, Brazil

[4]Department of Biological Sciences, California State University, San Marcos, CA, USA

[5]Programa de Pós-Graduação em Gestão de Risco e Desastre na Amazônia, Universidade Federal do Pará, Belém-PA, Brazil

Contents of this file

Corresponding author: G. L. Vourlitis, Department of Biological Sciences, California State University, San Marcos, CA, USA (georgev@csusm.edu)

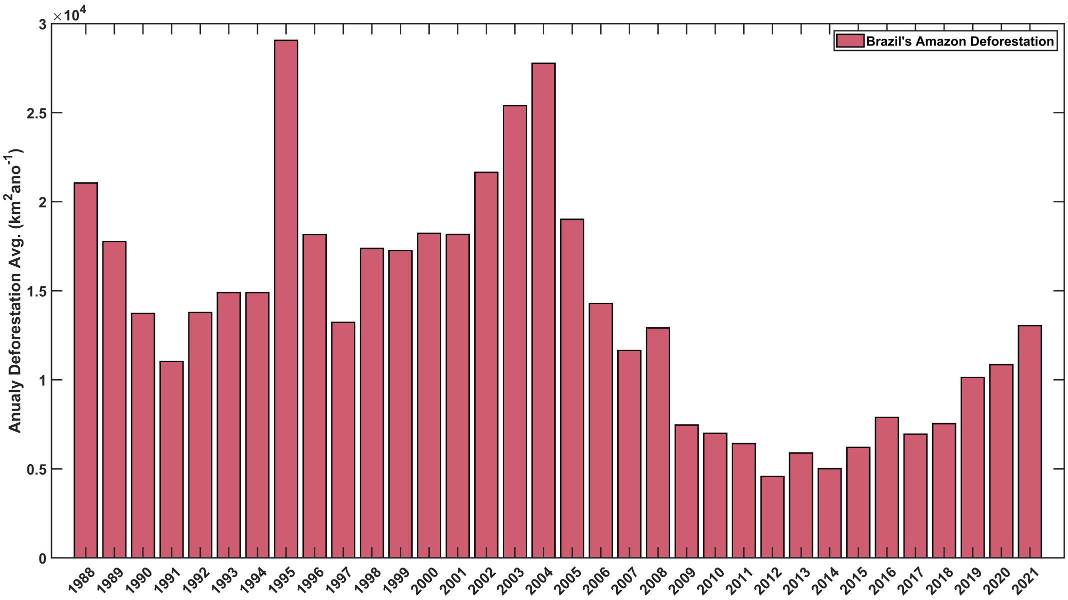

Figure S1. Time series of clear-cut deforestation in the Legal Amazon (1988 to 2021). Data originated from the PRODES project. The data were collected at the website from The National Institute for Space Research (INPE), link below (Table S3).

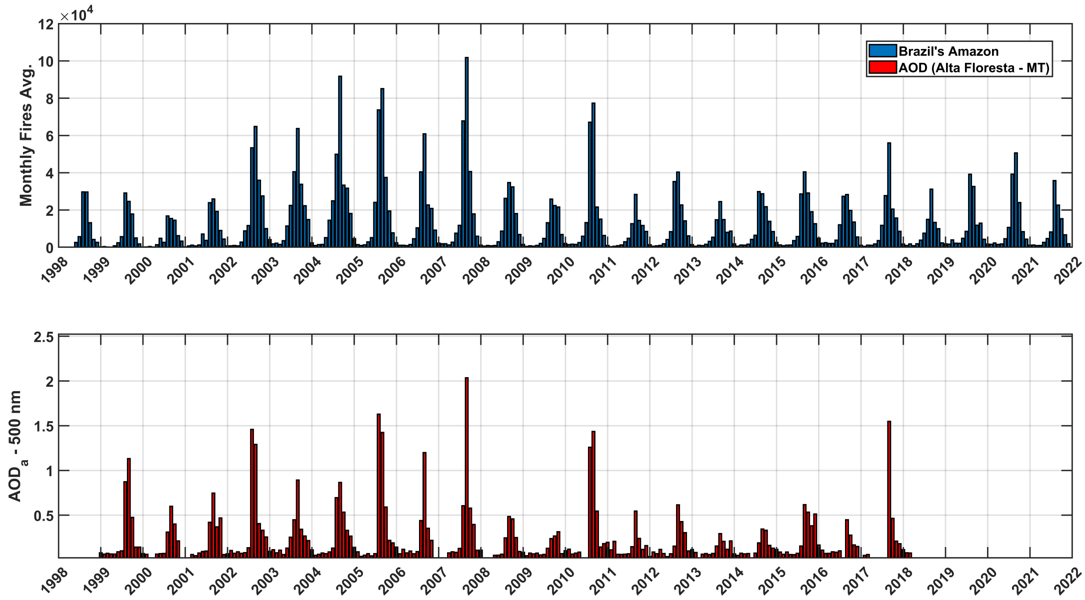

Figure S2. Shows the time series of fires in the Legal Amazon from 1998 to 2022 (top panel). Data originated from the PRODES project (link above mentioned). In the image below (bottom panel), we show the time series of aerosol optical depth for the Legal Amazon (1999 to 2018) originated from two remote sensors: MODIS from the AQUA and TERRA satellites and from the AERONET solar photometer (on the ground). All these remote measurements are managed by NASA, link below (Table S3).

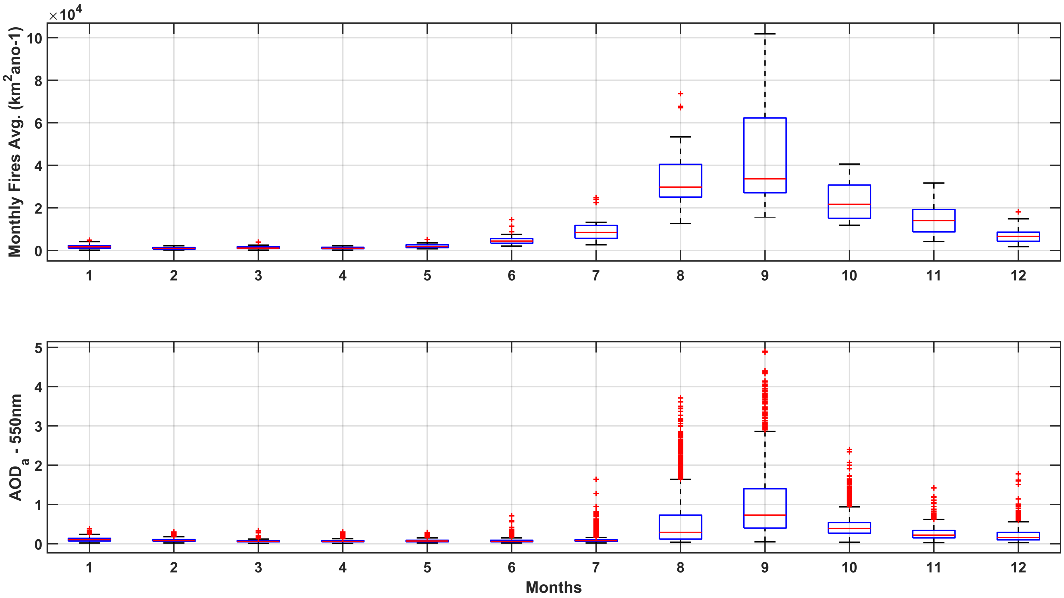

Figure S3. In the image above, the boxplot shows the statistical behavior of the time series of monthly data on fires that occurred in the Legal Amazon (1998 to 2022), observing the expressive seasonality during months August to November with a high peak of occurrence during months September. In the image below, the AOD boxplot tracks the fire behavior for the same period, link below (Table S3).

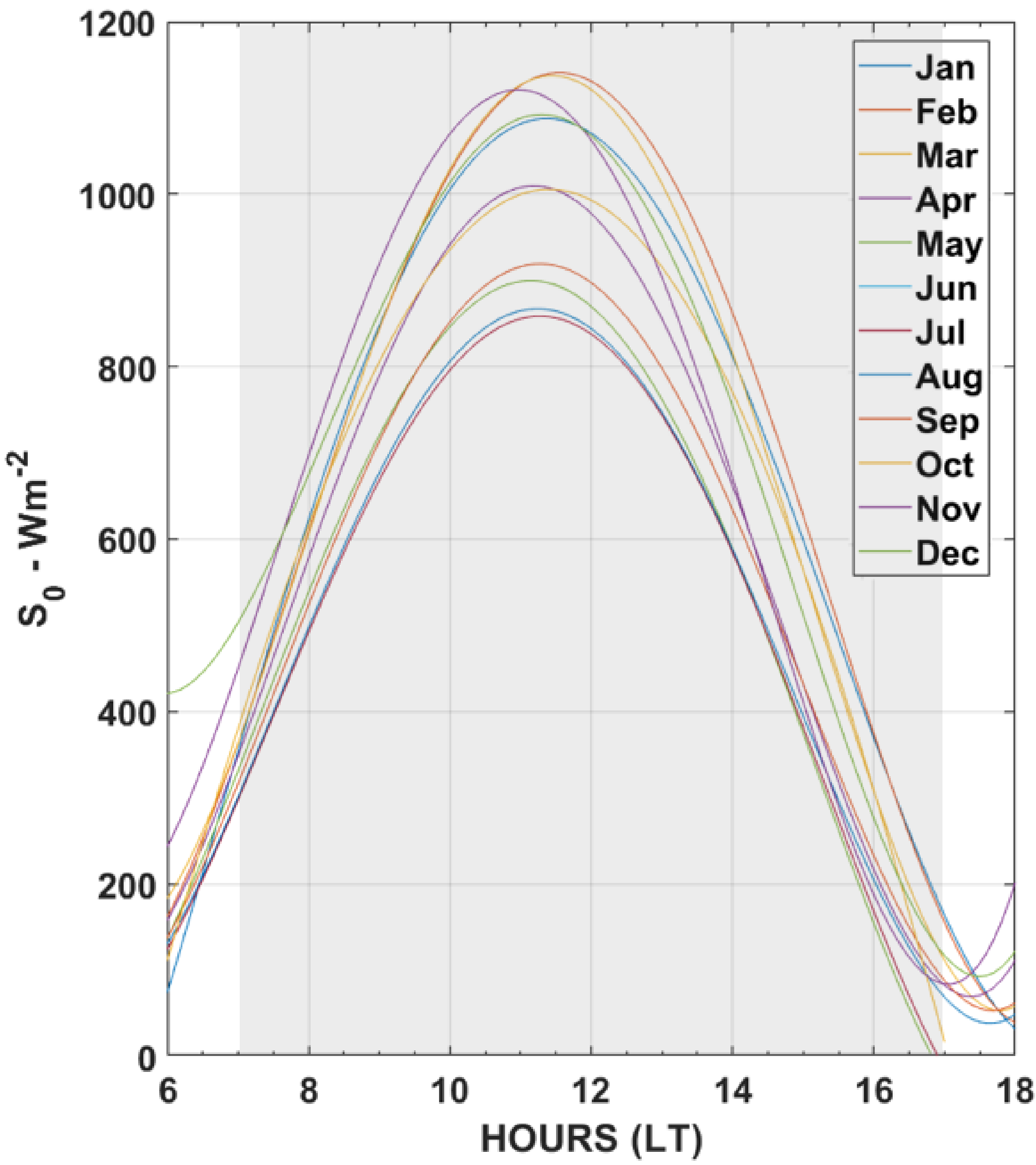

Figure S4. Curves containing the average hourly behavior (monthly) of incident solar radiation values measured by AERONET in Alta Floresta-MT. The analyzed hourly values are between 07h and 17h (LT) for the period from July 2005 to June 2008. We excluded from the data set all the values before 07h (LT) and after 17h (LT). Only the daylight hours are considered.

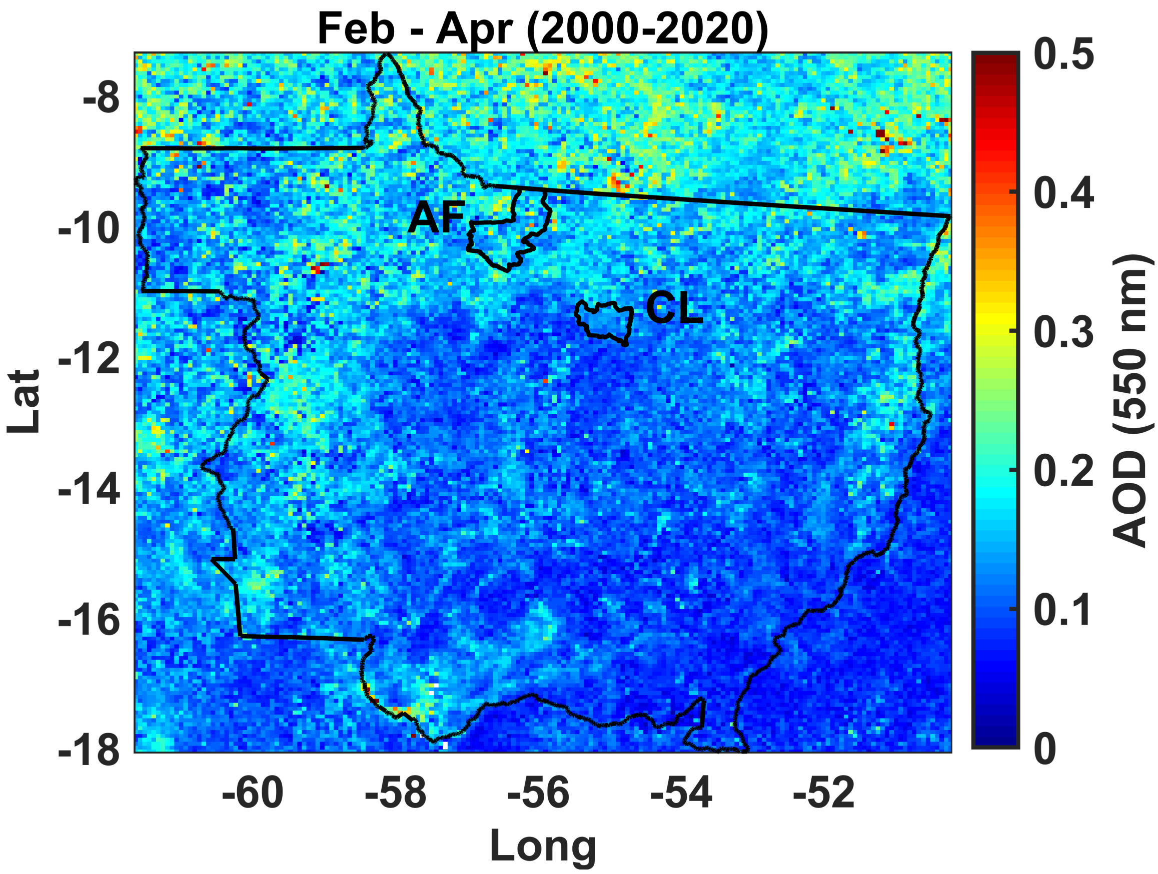

Figure S5. Spatial behavior of aerosol optical depth (AOD) over the State of Mato Grosso (intense area of the arc of deforestation). In the image above is the behavior of AOD during the wet season (February to April) for the data period from 2000 to 2020, obtained from the AQUA and TERRA Satellites (Table S3).

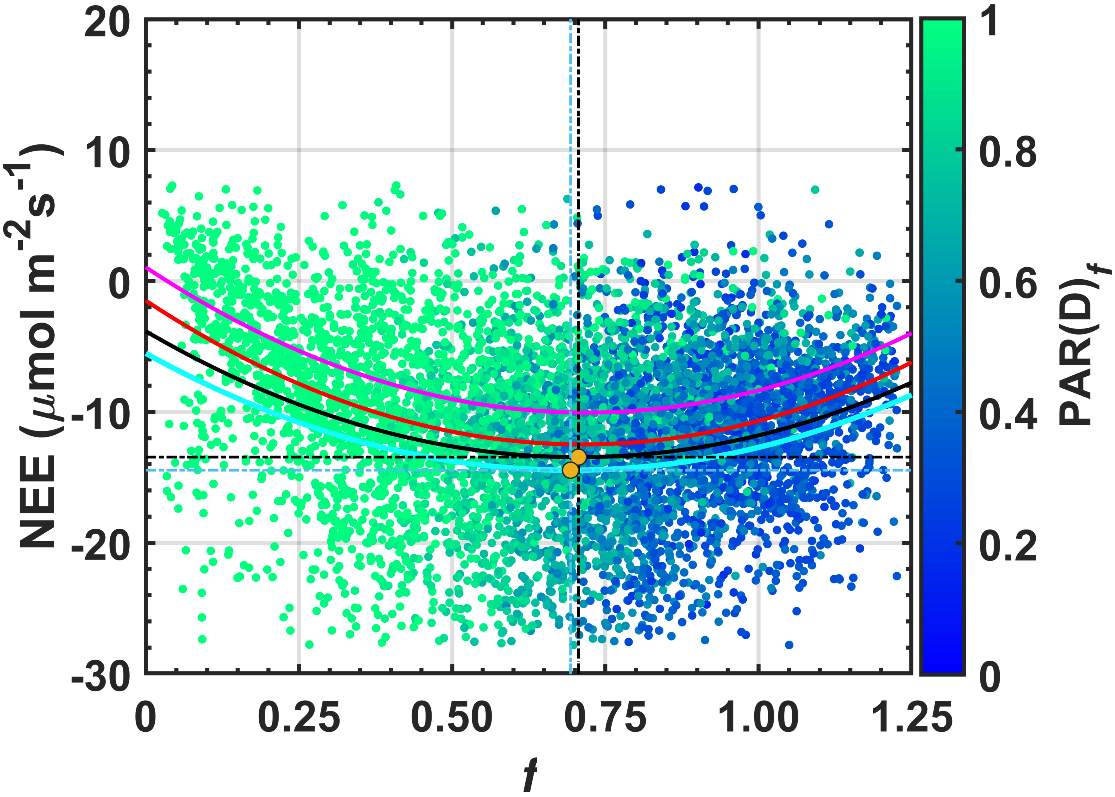

Figure S6. Variability of NEE for various SZA ranges, respectively equal to 0-20 (magenta), 20-40 (black), 40-60 (cyan), and 0-60 (red) degrees, in the semi-deciduous forest in the Claudia municipality, 50 km northeast of Sinop-MT (2005-2008). These graphs include the effects of aerosols in the experimental area.

Table S1. Coefficients of the fitted curves of the average hourly (monthly) data of incident solar radiation values measured by AERONET in Alta Floresta-MT. The analyzed hourly values are between 07h and 17h (LT) for the period from July 2005 to June 2008.

4th degree polynomial curves					
Months	$p1$	$p2$	$p3$	$p4$	$p5$
January	$+0.38$	-17	$+2.4\times10^2$	-1.1×10^3	$+1.2\times10^3$
February	$+0.57$	-26	$+4.1\times10^2$	-2.4×10^3	$+4.7\times10^3$
March	$+0.69$	-32	$+4.9\times10^2$	-3.0×10^3	$+6.2\times10^3$
April	$+0.64$	-29	$+4.3\times10^2$	-2.5×10^3	$+5.0\times10^3$
May	$+0.44$	-20	$+2.9\times10^2$	-1.6×10^3	$+2.8\times10^3$
June	$+0.43$	-20	$+3.0\times10^2$	-1.7×10^3	$+3.1\times10^3$
July	$+0.49$	-22	$+3.3\times10^2$	-1.9×10^3	$+3.6\times10^3$
August	$+0.51$	-23	$+3.5\times10^2$	-2.0×10^3	$+3.8\times10^3$
September	$+0.15$	-07	$+8.8\times10^1$	-1.4×10^2	-8.7×10^2
October	$+0.77$	-34	$+5.1\times10^2$	-2.9×10^3	$+5.8\times10^3$
November	$+0.74$	-35	$+5.5\times10^2$	-3.5×10^3	$+8.1\times10^3$
December	-0.42	$+24$	-5.1×10^2	$+4.9\times10^3$	-1.6×10^4

Table S2. Polynomial adjustments, coefficients, and statistics for the morning and afternoon periods between (07-17h) in the micrometeorological tower 50 km from Sinop-MT, in the municipality of Cláudia-MT, between 2005-2008.

Settings	**Angles**		**Coeficientes**		**Statistic**
Poly fit 2nd	SZA	a	b	c	Cp (x_v, y_v)
	0-20°	$+19$	-26	-5.5	$(0.68, -14.39)$
NEE	20-40°	$+19$	-27	-3.8	$(0.71, -13.39)$
	40-60°	$+21$	-31	$+1.0$	$(0.73, -10.44)$
	0-60°	$+22$	-31	-1.5	$(0.70, -12.42)$

Table S3. List with hyperlinks and Digital Object Identifiers (DOI) of all figures and tables used in this publication.

Open Research - Data Availability Statement				
Secondary Data	**Cloud-based Repository**	**Hyperlink**	**DOI**	**WebPage**
Remote Sensing (Satellites)	Terra-Aqua	Laads Daac	–	NASA Laads Daac
Remote Sensing (Ground)	Aeronet (Lev.2.0)	Goddard-Sfc	–	NASA Goddard
Short Wave Radiation	Aeronet (Lev.1.5)	Goddard-Sfc	–	NASA Goddard
Deforestation and fires	Prodes	Terra-Brasilis	–	INPE Prodes
Weather forecasts Models	Sol-Calculator	Solar-Calc	–	Meteo Exploration
Primary Data	**Cloud-based Repository**	**Hyperlink**	**DOI**	**Managers**
Eddy Flux (CO_2)	Mendeley Data	Brazil-EFlux-Stf	10.17632/m5h5fw872g.1	Cirino, G. et al. (2022)
Net Ecosystem Exchange (NEE)	Mendeley Data	Brazil-NFlux-Stf	10.17632/m5h5fw872g.1	Cirino, G. et al. (2022)
Meteorological Data	Mendeley Data	Brazil-AWsta-Stf	10.17632/m5h5fw872g.1	Cirino, G. et al. (2022)